© 2017. Published by The Company of Biologists Ltd | Development (2017) 144, 1566-1577 doi:10.1242/dev.138248

RESEARCH ARTICLE

Helios expression coordinates the development of a subset of striatopallidal medium spiny neurons

Raquel Martín-Ibáñez[1,2,3,4,5,], Mónica Pardo[1,2,3,4,**,*], Albert Giralt[3,4,6,‡], Andrés Miguez[1,2,3,4], Inés Guardia[1,2,3,4], Lucile Marion-Poll[7,§], Cristina Herranz[1,2,3,4,5], Miriam Esgleas[1,3,4,¶], Gerardo Garcia-Díaz Barriga[2,3,4,6], Michael J. Edel[8,9,10], Carlos Vicario-Abejón[4,11], Jordi Alberch[2,3,4,*], Jean-Antoine Girault[7], Susan Chan[1,2], Philippe Kastner[12,13] and Josep M. Canals[1,2,3,4,5,‡‡]**

ABSTRACT

Here, we unravel the mechanism of action of the Ikaros family zinc finger protein Helios (He) during the development of striatal medium spiny neurons (MSNs). He regulates the second wave of striatal neurogenesis involved in the generation of striatopallidal neurons, which express dopamine 2 receptor and enkephalin. To exert this effect, He is expressed in neural progenitor cells (NPCs) keeping them in the G_1/G_0 phase of the cell cycle. Thus, a lack of He results in an increase of S-phase entry and S-phase length of NPCs, which in turn impairs striatal neurogenesis and produces an accumulation of the number of cycling NPCs in the germinal zone (GZ), which end up dying at postnatal stages. Therefore, *He*$^{-/-}$ mice show a reduction in the number of dorso-medial striatal MSNs in the adult that produces deficits in motor skills acquisition. In addition, overexpression of *He* in NPCs induces misexpression of DARPP-32 when transplanted in mouse striatum. These findings demonstrate that He is involved in the correct development of a subset of striatopallidal MSNs and reveal new cellular mechanisms for neuronal development.

KEY WORDS: Ikaros, Neurogenesis, Medium spiny neurons, Cell cycle, Cell death, Ikzf2

INTRODUCTION

The mammalian striatum controls body movements through a sophisticated neuronal network that is dependent on the neurogenesis of two major classes of striatal neurons: the striatal projection neurons (or medium spiny neurons; MSNs) and the interneurons. MSNs are subdivided into two subpopulations: neurons that constitute the direct (or striatonigral) pathway and preferentially express substance P (SP) and D1R (dopamine receptor 1; DRD1), and neurons of the indirect (or striatopallidal) pathway, which mainly express enkephalin (ENK) and D2R (dopamine receptor 2; DRD2) (Gerfen, 1992). These two populations are differentially distributed within the striatal compartments. Striatal patches or striosomes mainly contain SP^+ MSNs, but both MSN subpopulations, SP^+ and ENK^+, are located in the matrix (Gerfen, 1992).

During embryonic development, radial glial cells (RGCs) from the ventricle wall of the lateral ganglionic eminence (LGE) undergo successive divisions to expand the pool of neural progenitor cells (NPCs), thereby increasing the volume of the germinal zone (subventricular zone; SVZ) (for reviews, see Götz and Barde, 2005; Merkle and Alvarez-Buylla, 2006). At certain developmental stages, NPCs differentiate into immature neurons that migrate radially to the mantle zone (MZ) (Götz and Barde, 2005; Merkle and Alvarez-Buylla, 2006; Mérot et al., 2009). Two waves of striatal neurogenesis segregate MSNs into two principal compartments: the patches, generated during the first neurogenic wave [starting at embryonic day (E) 12.5 in mouse]; and the matrix, developed during late striatal neurogenesis (starting at E14.5 in mouse) (Gerfen, 1992; Mason et al., 2005).

Within the LGE, transcription factors such as Gsx1 and Gsx2 (formerly named Gsh1 and Gsh2), Ascl1 (formerly named Mash1) and members of the Dlx family display specific patterns of expression within the GZ and the MZ, and they have been implicated in LGE patterning and/or differentiation (Eisenstat et al., 1999; Rallu et al., 2002; Waclaw et al., 2009; Yun et al., 2002). In addition, the transcription factors Ebf1, Isl1, Ctip2 (also known as Bcl11b), and Ikaros family members are mainly expressed in the MZ of the LGE where they regulate terminal differentiation of

[1]Stem Cells and Regenerative Medicine Laboratory, Production and Validation Center of Advanced Therapies (Creatio), Department of Biomedical Sciences, Faculty of Medicine and Health Sciences, University of Barcelona, 08036 Barcelona, Spain. [2]Neuroscience Institute, University of Barcelona, 08036 Barcelona, Spain. [3]August Pi i Sunyer Biomedical Research Institute (IDIBAPS), 08036 Barcelona, Spain. [4]Networked Biomedical Research Centre for Neurodegenerative Disorders (CIBERNED), Spain. [5]Research and Development Unit, Production and Validation Center of Advanced Therapies (Creatio), Faculty of Medicine and Health Sciences, University of Barcelona, 08036 Barcelona, Spain. [6]Pathophysiology of Neurodegenerative Diseases Laboratory, Production and Validation Center of Advanced Therapies (Creatio), Department of Biomedical Sciences, Faculty of Medicine and Health Sciences, University of Barcelona, 08036 Barcelona, Spain. [7]Inserm UMR-S839; Université Pierre et Marie Curie (UPMC, Paris 6), Sorbonne Universités; Institut du Fer à Moulin, 75005 Paris, France. [8]Control of Pluripotency Laboratory, Department of Biomedical Sciences, Faculty of Medicine and Health Science, University of Barcelona, 08036 Barcelona, Spain. [9]Victor Chang Cardiac Research Institute, Sydney, New South Wales, 2010 Australia. [10]School of Medicine and Pharmacology, Anatomy, Physiology and Human Biology, CCTRM, University of Western Australia, Western Australia, 6009 Australia. [11]Departamento de Neurobiología Molecular, Celular y del Desarrollo, Instituto Cajal, Consejo Superior de Investigaciones Científicas (CSIC), 28002 Madrid, Spain. [12]Department of Functional Genomics and Cancer, Institut de Génétique et de Biologie Moléculaire et Cellulaire (IGBMC), Inserm U964, Centre National de la Recherche Scientifique (CNRS) UMR 7104, 67400 Illkirch-Graffenstaden, France. [13]Faculté de Médecine, Université de Strasbourg, 67081 Strasbourg, France.

*Present address: Developmental Neurobiology and Regeneration Group, Department of Cell Biology, University of Barcelona, Barcelona, Spain. ‡Present address: Inserm UMR-S839; Université Pierre et Marie Curie (UPMC, Paris 6), Sorbonne Universités; Institut du Fer à Moulin, Paris, France. §Present address: Institut Curie, PSL Research University, CNRS UMR3215, Inserm U934, Mammalian Developmental Epigenetics group, Paris, France. ¶Present address: Institute of Stem Cell Research, Helmholtz Center Munich, Munich, Germany. **These authors contributed equally to this work

‡‡Author for correspondence (jmcanals@ub.edu)

J.M.C., 0000-0001-6829-7670

This is an Open Access article distributed under the terms of the Creative Commons Attribution License (http://creativecommons.org/licenses/by/3.0), which permits unrestricted use, distribution and reproduction in any medium provided that the original work is properly attributed.

Received 5 April 2016; Accepted 3 March 2017

Development (2017) 144, 1566-1577 doi:10.1242/dev.138248

striatal projection neurons (Arlotta et al., 2008; Ehrman et al., 2013; Garcia-Dominguez et al., 2003; Garel et al., 1999; Lobo et al., 2006, 2008; Martín-Ibáñez et al., 2010).

Ikaros family members are transcription factors that play essential roles during lymphocyte development (Cobb and Smale, 2005; Georgopoulos, 2002; Yoshida and Georgopoulos, 2014). Ikaros is the founder member of this family of DNA-binding proteins, which consists of Ikaros, Helios (He), Aiolos, Eos and Pegasus (Ikzf1-5, respectively – Mouse Genome Informatics) (John et al., 2009; Rebollo and Schmitt, 2003; Yoshida and Georgopoulos, 2014). In addition, Ikaros has been implicated in CNS development (Agoston et al., 2007; Alsiö et al., 2013; Martín-Ibáñez et al., 2010). We have recently described that He is also implicated in striatal development (Martín-Ibáñez et al., 2012). Within the LGE, *He* is expressed from E14.5 to postnatal day (P) 15 in both the GZ and the MZ, and its expression is downstream of *Gsx2* and *Dlx1/2* (Martín-Ibáñez et al., 2012). However, little is known about mechanisms of action of He during this developmental process.

Here, we demonstrate that *He* is expressed by NPCs at the G_0/G_1-phase of the cell cycle and induces neuronal differentiation by decreasing the levels of cyclin E and blocking the progression of these NPCs into S phase. Consequently, in the absence of *He*, proliferating NPCs accumulate in the GZ and the number of *Ctip2*$^+$ and DARPP-32 (PPP1R1B)$^+$ MSNs is reduced in the striatum resulting in disturbance of motor skill learning.

RESULTS

He loss induces aberrant striatal neurogenesis accompanied by de-regulation of NPC proliferation

Here, we demonstrated that He is expressed from E12.5 in scattered cells (Fig. S1) until P15 peaking at E18.5 (Martín-Ibáñez et al., 2012). He showed preferential expression in D2R-eGFP neurons (mean±s.e.m.: 46.69±8.37% of He$^+$ cells co-labeled with D2R; Fig. 1A; Fig. S2B) and *Penk* (preproenkephalin)$^+$ MSNs (89.05 ±5.77% of He$^+$ cells co-labeled with *Penk*; Fig. S3). In contrast, few D1R-eGFP$^+$ neurons and *Tac1* (tachykinin A, also known as tachykinin 1)$^+$ neurons co-expressed He (3.94±2.53% and 18.20 ±2.1% of He$^+$ cells co-labeled with D1R and *Tac1*, respectively; Fig. 1A; Fig. S2A; Fig. S3B,C). We next examined striatal birthdating in *He* knockout (*He*$^{-/-}$) and wild-type (wt) mice at different embryonic developmental stages (Fig. 1B-E). The first wave of striatal birthdating at E12.5 was not altered, as no differences were found in the total number of bromodeoxyuridine (BrdU)$^+$ cells between *He*$^{-/-}$ and wt mice (Fig. 1C). However, lack of *He* induced a significant reduction in the second wave of striatal birthdating at E14.5 (Fig. 1D). No significant differences were found between genotypes at E16.5 (Fig. 1E). This striatal birthdating impairment disturbed MSN generation as the density and total number of Ctip2-positive cells was decreased in *He*$^{-/-}$ mice compared with wt mice at E18.5 (Fig. 1F,G), suggesting a defect in the second neurogenic wave. In agreement, we observed that He$^+$ cells were mainly generated during the second wave of striatal neurogenesis (Fig. S4), between E14.5 (Figs. S4E-G) and E16.5 (Figs. S4H-J). Only a few cells were observed to be born at earlier stages (E13.5; Figs. S4B-D).

To assess whether He was expressed by proliferative cells in the LGE, we performed double staining for He and Ki67 (Mki67) at E16.5, BrdU or phospho-histone H3 (PH3) at E14.5. Our results showed that He$^+$ and Ki67$^+$ areas were mainly coincident at the GZ-MZ border at E16.5 (Fig. 2A). Within this area, He was expressed by NPCs expressing a low level of Ki67 (Fig. 2B,C) but not by cells expressing a high level of Ki67$^+$ (Fig. 2D; see Fig. S5 for quantification details). However, there was a lack of colocalization between He and short-pulsed BrdU NPCs (Fig. 2E,F), and He and PH3$^+$ NPCs (Fig. 2G,H). Interestingly, He only colocalized with Ki67-expressing cells during the neurogenic period as we could not observe colocalization from E18.5 onwards (Fig. S6).

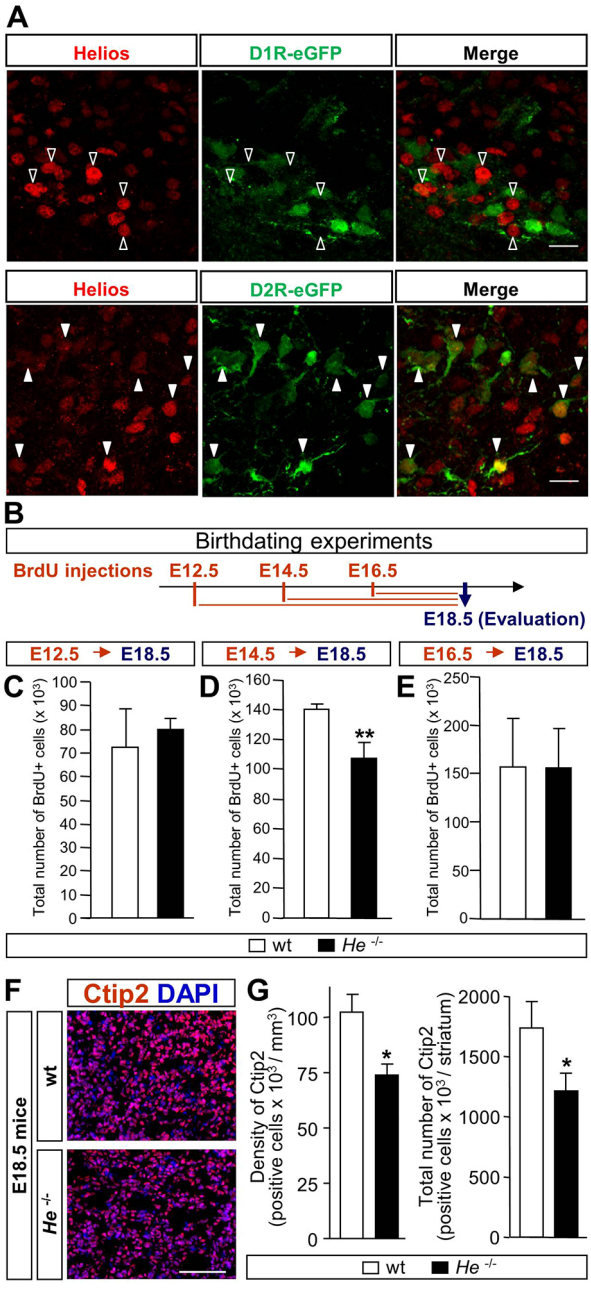

Fig. 1. *He* is necessary for the second wave of striatal neurogenesis. (A) Double immunohistochemistry against He and GFP in the D1R-eGFP mice and in the D2R-eGFP mice (images show DLS and VLS, respectively). Unfilled arrowheads show single-labeled cells and filled arrowheads show double-positive cells. Scale bars: 15 µm. (B) Schematic timeline of birthdating experiments performed in *He*$^{-/-}$ or wt mice. (C) No differences in neurogenesis were detected at E12.5 between *He*$^{-/-}$ and wt mice. (D) *He*$^{-/-}$ mice exhibited lower levels of neurogenesis than wt mice at E14.5. (E) No differences in neurogenesis were detected at E16.5 between *He*$^{-/-}$ and wt mice. (F) Representative images of Ctip2$^+$ neurons in the E18.5 (mid-striatal primordium is shown). Scale bar: 120 µm. (G) Quantification of the density and total number of Ctip2$^+$ cells in the whole striatal primordium reveals a significant reduction in *He*$^{-/-}$ mice compare with wt mice. Results represent the mean± s.e.m. of 4-5 mice per condition. Statistical analysis was performed using Student's *t*-test; **P*<0.05, ***P*<0.005.

Development (2017) 144, 1566-1577 doi:10.1242/dev.138248

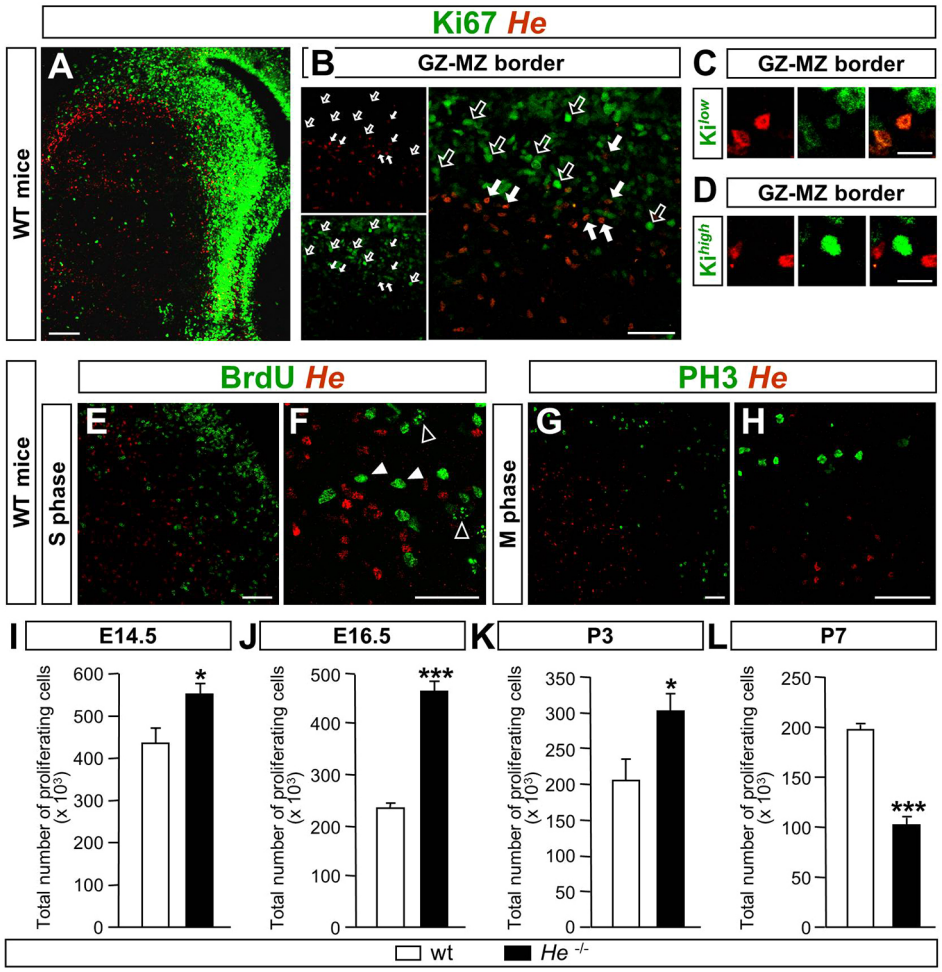

Fig. 2. He is expressed in NPCs at G_1 cell cycle phase and regulates their proliferation. (A) E16.5 striatal primordium, double stained against Ki67 and He. He^+ and $Ki67^+$ cells are coincident at the GZ-MZ border. Scale bar: 200 µm. (B) High magnification image of Ki67-He double immunohistochemistry at the dorsal striatal primordium shows that some cells are double positive at the GZ-MZ border. Filled arrows indicate double-positive cells and unfilled arrows point to Ki67 single-labeled cells. Scale bar: 50 µm. (C,D) At the GZ-MZ border, cells expressing a low level of Ki67 (Ki^{low}) express He (C), whereas cells expressing a high level of Ki67 (Ki^{high}) do not express He (D). Scale bars: 20 µm. (E,F) Double staining for BrdU and He shows that cells in S phase are not positive for He at E14.5 in the dorsomedial LGE. (E) High magnification picture shows that although He^+ and $BrdU^+$ cells are located in the same area, they do not colocalize. (F) Unfilled arrowheads indicate $BrdU^+$ cells that have recently entered S phase as shown by the appearance of transcription units; filled arrowheads indicate cells that incorporated BrdU at more advanced cell cycle stages. Scale bars: 50 µm. (G,H) There is no coincidence between He-expressing cells and cells in M phase as detected by PH3 staining; low (G) and high (H) magnification images of DMS are shown. Scale bars: 50 µm. (I-L) Quantification of the total number of proliferating cells in the whole GZ show that lack of *He* induces a significant increase at E14.5 (I), E16.5 (J) and P3 (K) and a significant decrease at P7 (L) compared with wt mice. Results represent the mean±s.e.m. of 5-7 mice per condition. Statistical analysis was performed using Student's *t*-test; $*P<0.05$, $***P<0.001$.

Analysis of the number of cycling cells at different developmental stages in $He^{-/-}$ and wt mice (Fig. 2I-L) showed that the total number of proliferating cells in the GZ was significantly increased from E14.5 to P3 (Fig. 2I-K), inducing an enlargement of the proliferative area stained with Ki67 (Fig. S7). Interestingly, this feature reverted at P7, when the number of proliferating cells in $He^{-/-}$ mice decreased with respect to wt mice (Fig. 2L; Fig. S8). To analyze whether a specific subpopulation of progenitors was more compromised than others, we counted the percentage of $PH3^+$ basal, subapical and apical progenitors as described by Pilz et al. (2013) (Fig. S9A,B). No differences were found between $He^{-/-}$ and wt mice (Fig. S9B). We also analyzed by QPCR the expression of striatal progenitor markers at E16.5. No differences were found in the levels of mRNA for these markers in $He^{-/-}$ compared with wt mice (Fig. S9C).

To elucidate further the role of He in NPC proliferation, we performed loss-of-function (LOF) and gain-of-function (GOF) *in vitro* studies using a neurosphere assay (Fig. S10). There was an increase in the number of proliferating cells in the absence of *He* (Fig. S10A,C,E,F). Accordingly, *He* overexpression significantly reduced the number of proliferating NPCs with respect to the control eGFP overexpressing NPCs (Fig. S10B,D). In addition, in the absence of *He*, NPCs were less prone to differentiate to β-III-tubulin$^+$ neurons (Fig. S10H). In contrast, an increase in the number of neurons was observed after *He* overexpression (Fig. S10I-K). Interestingly, *He* did not exert any change in the percentage of $GFAP^+$ cells in the LOF or in the GOF experiments (Fig. S10H,I). Consequently, $He^{-/-}$ mice did not present any defects in astrocyte differentiation compared with wt mice (Fig. S11A-D). In fact, we did not observe colocalization between He and GFAP (Fig. S11E).

Development (2017) 144, 1566-1577 doi:10.1242/dev.138248

He controls proliferation through regulation of the G_1-S checkpoint

To understand the cellular mechanism by which He regulates NPC proliferation and neurogenesis, we next analyzed the cell cycle. We observed that lack of *He* induced a significant increase in NPC S-phase length that, in turn, increased cell cycle length as measured by an accumulative exposure to BrdU (see Materials and Methods; Lange et al., 2009) (Fig. 3A,C). However, no differences were observed between the length of the G_2/M phases in NPCs derived from $He^{-/-}$ compared with wt mice, as determined by analysis of the mitotic BrdU labeling index as described previously (Takahashi et al., 1995) (Fig. 3B,C; Fig. S12). Representation of the percentage of cell cycle phases respect to the total cell cycle length clearly demonstrated an elongation of S-phase length when *He* was knocked down (Fig. 3C). Consistently, *He* overexpression induced a severe reduction of S-phase length (GOF; Fig. 3D). Our results also showed that in the absence of *He* more NPCs entered S phase (punctate $BrdU^+/EdU^+$; Fig. 3E-H) but the number of cells exiting S phase was not altered ($BrdU^+/EdU^-$; see 'S-phase analysis' in Materials and Methods; Lange et al., 2009) (Fig. 3E,F). In addition, no differences were found in the number of cells exiting the cell cycle ($BrdU^+/Ki67^-$; see 'Cell cycle index' in Materials and Methods; Urbán et al., 2010) in LOF (Fig. S13A,B,D) or GOF (Fig. S13C) experiments.

In order to demonstrate the mechanism by which He controls S-phase entry, we next analyzed the protein levels of cyclin E (Fig. 4), a key regulator of the transition from G_1 to S phase (Ohtsubo et al., 1995). NPCs derived from $He^{-/-}$ mice presented increased levels of PCNA, a marker of cell proliferation, and cyclin E (Fig. 4A-D). Accordingly, *He* overexpression (Fig. 4E-H) produced a reduction of PCNA and cyclin E protein levels (Fig. 4E-H), and a drastic reduction of cyclin E mRNA levels (Fig. 4J). Similarly, *in vivo* analysis showed that an increased number of NPCs had entered into S phase in the GZ of $He^{-/-}$ compared with wt mice (Fig. 4K), which was accompanied by increased protein levels of cyclin E in the LGE (Fig. 4L,M). Chromatin immunoprecipitation experiments performed by Kim and co-workers (Kim et al., 2015) demonstrated that He binds the cyclin E gene (*Ccne1*) promoter site and another site downstream of the gene (Fig. 4N). However, no changes of the two cyclin E regulators E2F1 and retinoblastoma (Rb; Rb1) (Harbour, 2000; Ohtani et al., 1995) were observed in NPCs derived from $He^{-/-}$ mice (Fig. S14). Altogether, these results suggest that He might control cell cycle progression through regulation of cyclin E expression.

Postnatal cell death is increased in $He^{-/-}$ mice

We next investigated whether cell death was altered in the absence of *He* during embryonic and postnatal stages. Cleaved caspase-3 immunohistochemistry did not reveal any differences between $He^{-/-}$ and wt mice at embryonic stages (E14.5, E16.5 and E18.5; data not shown). However, a significant increase in the number of apoptotic cells was detected in the GZ and the MZ at P3 in $He^{-/-}$ mice (Fig. 5A-D), which normalizes at P7 (Fig. 5E,F). To check whether cell death is related to a delay in the differentiation of NPCs, we applied an ethynyl deoxyuridine (EdU) pulse at E18.5 and double staining for EdU and cleaved caspase-3 (Fig. 5G) or neural markers (Fig. S15) at P3. EdU^+ apoptotic cells were found in the MZ of $He^{-/-}$ mice (Fig. 5H-K) and they were positive for the neuronal marker NeuN (Rbfox3) (71.3±7.10% of cleaved caspase-3^+ cells co-labeled with NeuN; Fig. S15). These results suggest that in the absence of *He* there is a delayed differentiation of NPCs, which subsequently die.

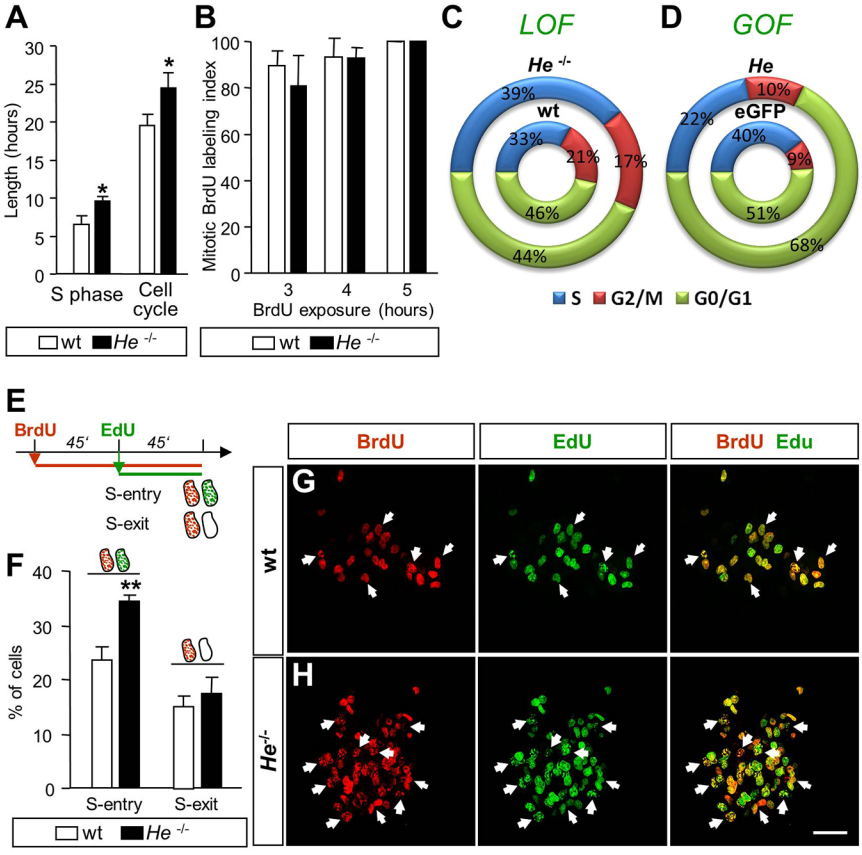

Fig. 3. *He* is necessary for cell cycle S-phase regulation. (A) $He^{-/-}$ mice-derived neurospheres exhibited an increase in the length of S phase and cell cycle compared with wt mice-derived neurospheres. (B) Mitotic BrdU labeling index, which is used to calculate G_2/M phase length, was the same in both wt and $He^{-/-}$ mice-derived neurospheres. (C,D) Schematic of the percentages of the length of the cell cycle phases with respect to the total cell cycle duration obtained from LOF (C) and GOF (D) experiments. (E) Schematic timeline of S-phase entry/exit experiments performed with a double pulse of BrdU and EdU in wt and $He^{-/-}$ mice-derived neurospheres. (F) A higher number of NPCs entered S phase in $He^{-/-}$ mice-derived neurospheres compared with wt mice-derived ones, whereas no differences were observed between both cultures in the number of cells that exit S phase. (G,H) Representative images of BrdU and EdU double staining performed in wt and $He^{-/-}$ mice-derived neurospheres. Arrows indicate double-positive cells. Scale bar: 50 µm. Results represent the mean±s.e.m. of 4-5 LGE-derived neurosphere cultures. Statistical analysis was performed using Student's *t*-test; $^*P<0.05$, $^{**}P<0.005$.

Development (2017) 144, 1566-1577 doi:10.1242/dev.138248

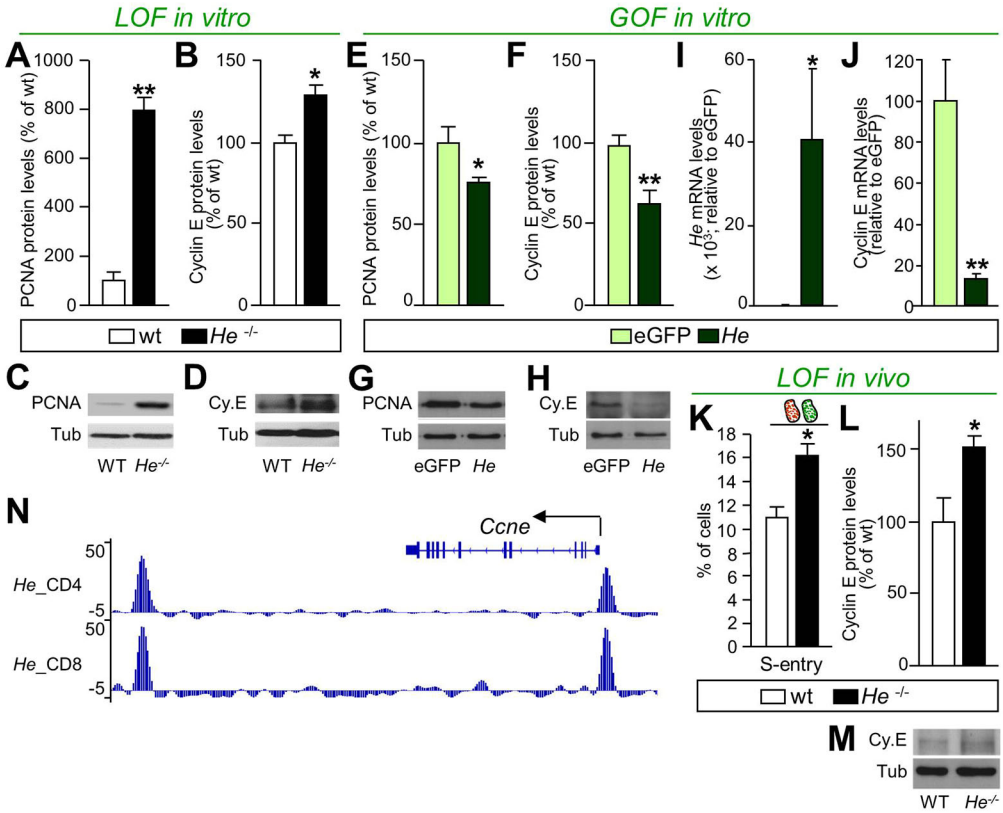

Fig. 4. He regulates cyclin E expression. (A-D) PCNA (A,C) and cyclin E (Cy.E; B,D) protein quantification show a significant increase in the levels of both proteins in $He^{-/-}$-derived neurospheres compared with wt neurospheres. Representative blots are shown for PCNA (C) and cyclin E (D). (E-H) By contrast, *He* overexpression induces a significant decrease in PCNA (E,G) and cyclin E (F,H) protein levels compared with the control eGFP. Representative blots are shown for PCNA (G) and cyclin E (H). (I) mRNA expression of *He* in neurosphere cultures overexpressing *He* or the control eGFP. (J) Cyclin E mRNA levels are downregulated in *He* overexpressing neurospheres compared with the control eGFP. (K) *In vivo* analysis shows an increased percentage of cells entering into S phase in $He^{-/-}$ LGEs compared with wt at E14.5. (L,M) Quantification of $He^{-/-}$ and wt E14.5 LGEs indicates significantly increased protein expression of cyclin E in the absence of *He*. (M) Representative blots are shown for cyclin E in LOF *in vivo* experiments. (N) Cumulative counts peak graph from the chip-Seq analysis of *He* interaction. The cyclin E (*Ccne1*) gene region shows two prominent hits one within the proximal promoter region, and one downstream of the gene. Tubulin (Tub) was used as loading control for western blots. For *in vitro* studies, results represent the mean±s.e.m. of 4-5 LGE-derived neurosphere cultures. RT-PCR results represent the mean±s.e.m. of 4-5 independent samples and are expressed relative to control eGFP, considered as 100%. For *in vivo* studies, results represent the mean±s.e.m. of 4-5 LGEs. Statistical analysis was performed using Student's *t*-test; **P*<0.05, ***P*<0.005.

He is necessary for MSN development

We next characterized the striatum of $He^{-/-}$ adult mice. First, we studied brain hemisphere volume and detected a slight decrease in $He^{-/-}$ mice compared with wt mice (Fig. S16A,C; 8.36% decrease). Interestingly, characterization of striatal volume revealed a larger and significant reduction in $He^{-/-}$ compared with wt mice (Fig. S16B,C; 20.17% decrease). The ratio of striatal versus hemisphere volume showed that striatal volume is selectively disturbed in $He^{-/-}$ mice (wt, 18.23±0.79%; $He^{-/-}$, 15.45±0.60%), showing a 15.24% reduction of relative striatal volume. Stereological analysis of calbindin$^+$ and DARPP-32$^+$ neurons revealed a significant decrease in the density (Fig. S16D,E,H,I) and total number of MSNs in the striatum of $He^{-/-}$ compared with wt mice (Fig. 6A,B). We also analyzed the density of DARPP-32$^+$ neurons in different striatal areas including the dorso-medial striatum (DMS), dorso-lateral striatum (DLS), ventro-medial striatum (VMS) and ventro-lateral striatum (VLS) (Fig. 6K). These experiments demonstrated a significant decrease only in the DMS in $He^{-/-}$ mice compared with wt mice (Fig. 6E-H). Interestingly, a specific alteration of the ENK$^+$ population was also observed in the DMS in the absence of *He* (Fig. 6I). However, no differences were found for the SP$^+$ population in $He^{-/-}$ mice compared with wt mice (Fig. 6J). In addition, no differences were observed between genotypes in the cholinergic and parvalbumin$^+$ striatal interneurons (Fig. S16F,G; Fig. 6C,D).

In order to study the direct involvement of He in the acquisition of a mature MSN phenotype, we transplanted eGFP or *He*-overexpressing NPCs into the mouse neonatal forebrain (Fig. 7A). Compared with control cells, *He*-overexpressing cells displayed more robust branching 2 weeks post-transplantation (total neurite tree length per neuron: GFP 168.13± 21.92 µm, *He* 413.66±98.84 µm, *P*=0.0046; number of branches per neuron: GFP 14.43±1.68, *He* 24.89±4.08, *P*=0.0089; Fig. 7B-E) and DARPP-32 expression was observed in few scattered cells adjacent to the striatum (Fig. 7G,H). Four weeks post-transplantation, several *He*-overexpressing cells displayed DARPP-32 expression (Fig. 7J-L), in contrast to control cells, which were all DARPP-32 negative (Fig. 7I). Quantification of DARPP-32$^+$ neurons in GFP transplanted cells demonstrated a 150-fold increase in the number of double-stained cells in He-expressing cells compared with controls. In addition, *He* overexpression in striatal primary cultures significantly increased the number of calbindin$^+$, DARPP-32$^+$ and ENK$^+$ cells (Fig. S17).

He loss disturbs the acquisition of motor skills

To analyze the functional implication of *He* loss, we assessed the performance of motor tasks in wt and $He^{-/-}$ mice (Fig. 8). In the

Development (2017) 144, 1566-1577 doi:10.1242/dev.138248

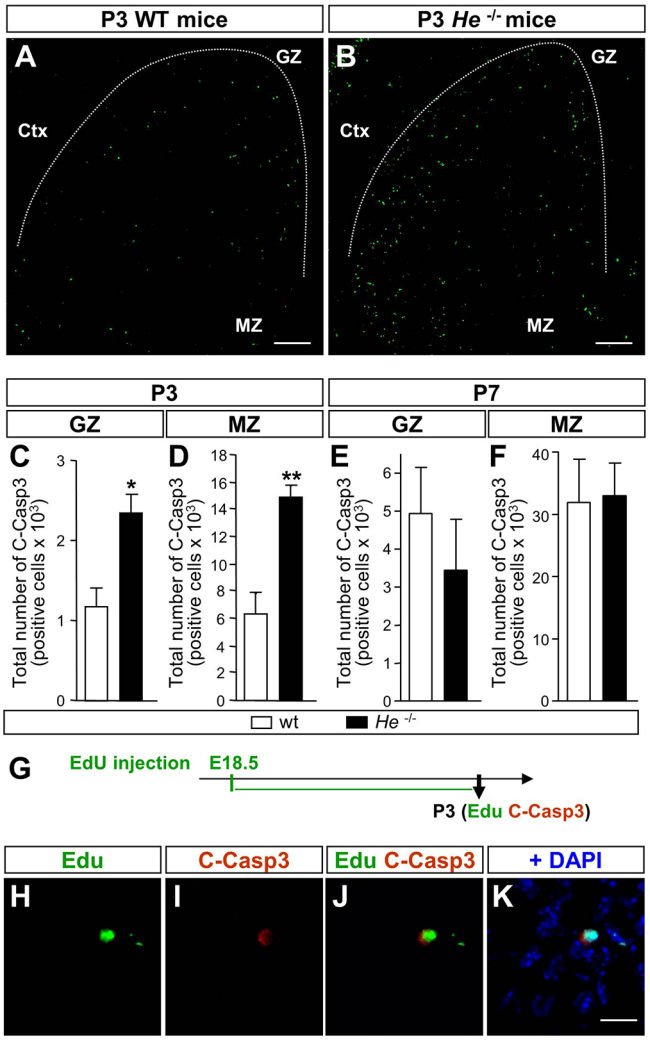

Fig. 5. *He* knockout mice exhibit increased programmed cell death at postnatal stages. (A,B) Representative photomicrographs corresponding to P3 striatal coronal sections from wt (A) and $He^{-/-}$ (B) mice immunostained for cleaved caspase 3. Scale bars: 200 µm. Ctx, cortex. (C) Lack of *He* induces a significant increase in the total number of cleaved caspase-3 (C-Casp3)$^+$ cells in the GZ at P3. (D) $He^{-/-}$ mice exhibited an increase in the total number of C-Casp3$^+$ cells in the MZ at P3 compared with wt mice. (E,F) No differences in the total number of C-Casp3$^+$ cells were observed between genotypes in the GZ (E) or in the MZ at P7 (F). (G) Injection of EdU at E18.5 and recovery of the $He^{-/-}$ pups at P3 permitted the examination of whether cells that exit the cell cycle after E18.5 and migrate to the striatum MZ are positive for C-Casp3. (H-K) Representative photomicrographs of striatal coronal ventral section showing colocalization of EdU and C-Casp3. Scale bar: 30 µm. Results represent the mean±s.e.m. of 4-5 mice per condition. Statistical analysis was performed using Student's *t*-test; **P*<0.05, ***P*<0.005.

simple swimming test, $He^{-/-}$ mice displayed significant abnormalities compared with wt mice in their swimming latency in the first testing trial (genotype: $F_{2,162}$=4.08, P<0.05; post-hoc trial 1: P<0.01), but these disappeared over subsequent trials (Fig. 8A).

In addition, wt and $He^{-/-}$ mice progressively improved their performance in the balance beam along four trials (trial: $F_{3,112}$=14.66, P<0.001). However, $He^{-/-}$ mice fell off more times than controls during the first trials (genotype: $F_{2,112}$=13.52, P<0.01; post-hoc trial 1: P<0.001; post-hoc trial 2: P<0.01; Fig. 8B).

In the rotarod test, all mice reached a stable level of performance within six trials (Fig. 8C), as measured by a decrease in the number of falls in 60 s per mouse (testing trial $F_{5,138}$=15.87, P<0.01). However, acquisition on the rotarod task was significantly delayed in $He^{-/-}$ compared with wt mice (genotype $F_{2,138}$=21.03, P<0.01).

DISCUSSION

Striatal MSNs are generated from NPCs located at the GZ of the LGE. Here, we show that He regulates late striatal neurogenesis that gives rise to D2R$^+$ ENK neurons. He is expressed by NPCs in the G_1/G_0 cell cycle phase at the GZ, impairing the G_1-S transition by the regulation of cyclin E, which in turn induces neuronal differentiation. Consequently, lack of *He* produces an extended S phase and cell cycle length that increases the number of proliferating NPCs at the GZ. At the beginning of the postnatal period, the number of these NPCs is reduced due to their late aberrant neurogenesis that results in cell death. These abnormalities of embryonic development in $He^{-/-}$ mice produce a reduction of a specific subset of striatopallidal neurons of the dorsomedial striatum that control motor skill learning.

He is necessary for striatopallidal neurogenesis

NPCs located at the GZ of the LGE become postmitotic and migrate into the MZ to acquire the MSN phenotype (Brazel et al., 2003). We have previously proposed a model for the development of striatal subpopulations in which Ikaros and He are involved in the development of striatopallidal ENK$^+$ matrix MSNs (Martín-Ibáñez et al., 2012). This hypothesis is reinforced by the localization of *He* in ENK$^+$ neurons that co-express D2R (present results). Besides the apparent similar function between He and Ikaros on ENK$^+$ neurogenesis, there is much evidence that they determine different ENK$^+$ subpopulations. They are expressed by different cells (Martín-Ibáñez et al., 2012), and their expression is not modified in the reciprocal knockout mice (Martín-Ibáñez et al., 2010, 2012). These results are contrary to the role of Ikaros family members in the hematopoietic system where they directly interact (Hahm et al., 1998; John et al., 2009), suggesting specific mechanisms of action in each system.

He regulates neurogenesis through the control of the G1-S phase checkpoint

Gsx2$^+$ radial glial cells constitute the first NPCs that appear during LGE ontogeny, which differentiate with the onset of the neurogenesis from the neuroephithelial cells (for a review, see Dimou and Götz, 2014). *He*-expressing cells are derived from radial glial cells, as its expression disappears in *Gsx2* knockout mice (Martín-Ibáñez et al., 2012). However, *He* loss does not compromise the number of the radial glial cell subtypes described elsewhere (Pilz et al., 2013). Radial glial cells generate the large MSNs output by a series of intermediate NPCs to amplify specific lineages, although these striatal NPCs are still poorly characterized. *He* is expressed by a small number of NPCs distributed in deep SVZ. Although the localization of *He* is mainly at the dorsal areas, it does not seem to be defining a specific SVZ domain as it has been described for other transcription factors in the VZ (Flames et al., 2007).

Some of the NPCs that express *He* at the GZ co-express low levels of Ki67. Considering that Ki67 labels cells during all phases of the cell cycle except G_0 (Kanthan et al., 2010; Scholzen and Gerdes, 2000) and that G_1 is the cell cycle phase with lower Ki67 expression levels (Lopez et al., 1991), we hypothesized that *He* is expressed in a subset of NPCs during G_1 and G_0 phases. The lack of colocalization between *He* and BrdU or PH3 reinforces the idea that *He* is not expressed by cells at S or M phases, respectively. Within G_1 phase He impairs S-phase entry, reducing S-phase length and arresting

Development (2017) 144, 1566-1577 doi:10.1242/dev.138248

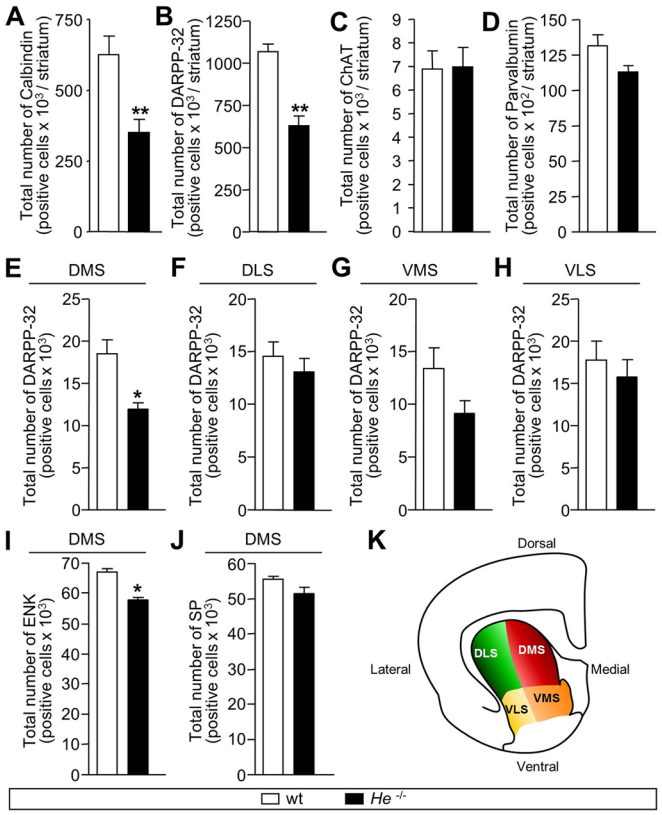

Fig. 6. Lack of *He* during development alters the number of mature MSNs in adult *He*$^{-/-}$ mice. (A-J) Stereological cell counts of neuronal striatal populations in wt and *He*$^{-/-}$ mice striatum. (A) The total number of striatal calbindin^{+} cells is reduced in *He*$^{-/-}$ adult mice compared with wt adult mice. (B) The total number of striatal DARPP-32^{+} cells is reduced in *He*$^{-/-}$ adult mice compared with wt adult mice. (C,D) The total number of striatal ChAT^{+} (C) or parvalbumin^{+} (D) cells is not altered between wt and *He*$^{-/-}$ adult mice. (E-H) The total number of striatal DARPP-32^{+} cells is specifically reduced in the DMS (E) in *He*$^{-/-}$ adult mice compared with wt adult mice. No differences are found in the DLS (F), VMS (G) and VLS (H) between both genotypes. (I) The total number of ENK^{+} cells is reduced in the DMS of *He*$^{-/-}$ compared with wt mice. (J) The total number of SP^{+} cells is not altered in the DMS between wt and *He*$^{-/-}$ mice. (K) Schematic showing the division of a coronal striatal section into DMS, DLS, VMS and VLS regions. Results represent the mean±s.e.m. of 4-5 mice per condition. Statistical analysis was performed by using Student's *t*-test; **P*<0.05, ***P*<0.005.

NPCs at G_1/G_0 phase to facilitate neuronal differentiation. Consequently, *He*$^{-/-}$ mice NPCs increase S-phase entry and continue proliferating in the striatal GZ impairing neurogenesis (see Fig. S18 for a representative scheme). Similarly, Lacomme and co-workers demonstrated that Ngn2 regulates G_1-S phase transition, blocking S-phase entry and increasing the number of NPCs at G_1/G_0 phase (Lacomme et al., 2012). In addition, NPCs shorten S phase on commitment to neuron production (Arai et al., 2011; Turrero García et al., 2015). Thus, cell cycle length and G_1-S phase transition are crucial processes for neurogenesis and both are regulated by He. We hypothesize that He arrests LGE-derived NPCs into phases G_1/G_0 to allow the accumulation of the protein machinery necessary for their differentiation to specific striatal neurons. In fact, crucial aspects of neural commitment are acquired in the final division cycle of NPCs. For example, the cortical laminar fate of NPC is acquired during the final progenitor cell division (Bohner et al., 1997; Edlund and Jessell, 1999; McConnell and Kaznowski, 1991). Similarly, during motor neuron development, NPCs become sonic hedgehog (Shh) dependent late in their final progenitor cell cycle (Ericson et al., 1996), which commits them to a motor neuronal fate (Tanabe et al., 1998).

G_1-S phase transition is regulated by Cdk2 and cyclin E, which form a complex that participates in G_1-S phase checkpoint (reviewed by Hardwick and Philpott, 2014; Ohtsubo and Roberts, 1993). Our results suggest that cyclin E is a key factor regulated by He that correlates with the G_1-S phase transition impairment observed in the *He*$^{-/-}$ mice. In fact, the cyclin E gene (*Ccne1*) has two very strong He-binding domains (Kim et al., 2015) suggesting a direct regulation. Similar to our results, Pilaz and colleagues described that overexpression of cyclin E in cortical NPCs promotes a proliferation increase whereas downregulation of cyclin E led to a decrease in progenitor proliferation (Pilaz et al., 2009). In addition, a direct correlation between cyclin E and S-phase entry was proposed by ectopic expression of cyclin E, which shortens the G_1 interval and increases the length of S phase by advancing G_1-S phase transition (Resnitzky et al., 1994). Furthermore, ectopic expression of cyclin E can drive G_1 cells into S phase under conditions in which Rb is not phosphorylated and E2F is not activated (Leng et al., 1997; Lukas et al., 1997). This is in agreement with our results, as we observed an increase in cyclin E but no alterations in phosphorylated RB or E2F in *He*$^{-/-}$ mice.

He loss increases postnatal cell death

The homeostasis of NPCs in the striatum is a regulated process in which neurogenesis precedes astro-gliogenesis during development (Alvarez-Buylla et al., 2001; Ninkovic and Götz, 2013). However, contrary to the increase of astro-gliogenesis observed in *Ikaros*$^{-/-}$ mice (Martín-Ibáñez et al., 2010), we could not detect any effects on glial cells in *He*$^{-/-}$ mice. The role of He in neurogenesis through cyclin E-mediated G1-S transition without modifying astro-gliogenesis coincides with the effect of deferoxamine, a G_1/S-phase blocker, which increases neuronal but not astrocytic NPC differentiation (Kim et al., 2006; Misumi et al., 2008).

The reduction of NPCs in *He*$^{-/-}$ mice at postnatal stages can be related to the increase in cell death during this period. Naturally occurring cell death is a crucial step in re-defining the final size of specific neuronal populations (Burek and Oppenheim, 1996; Kristiansen and Ham, 2014), which directly correlates with the time of prior exit from cell cycle and position during neuronal development (Gould et al., 1999). Our results point to the idea that the cell death observed in *He*$^{-/-}$ mice is a consequence of the delay in NPCs exiting cell cycle around E18.5, then migrating into the MZ where they become neurons and die. Therefore, lack of He produces a dysfunction in the time and position of late-generated neurons in the MZ. Dual effects have also been described for Isl1 and Ebf1, which promote differentiation of striatonigral neurons and in their absence striatal cell death is observed (Garel et al., 1999; Lu et al., 2014). Taken together, all these results indicate that He loss causes aberrant neurogenesis, which in turn induces neuronal cell death compromising striatal development.

He participates in the differentiation of a subset of MSNs that is involved in early motor learning

He-mediated regulation of the NPC cell cycle correlates with the determination of a subset of striatopallidal MSNs. The events occurring during striatal development of *He*$^{-/-}$ mice cause a specific reduction of striatal MSNs in the DMS in the adulthood. Taken together, our present findings demonstrate that He plays a direct role in the commitment of NPCs to MSNs. Accordingly, *He* overexpression is sufficient to differentiate NPCs transplanted into the striatum in MSNs expressing DARPP-32.

Development (2017) 144, 1566-1577 doi:10.1242/dev.138248

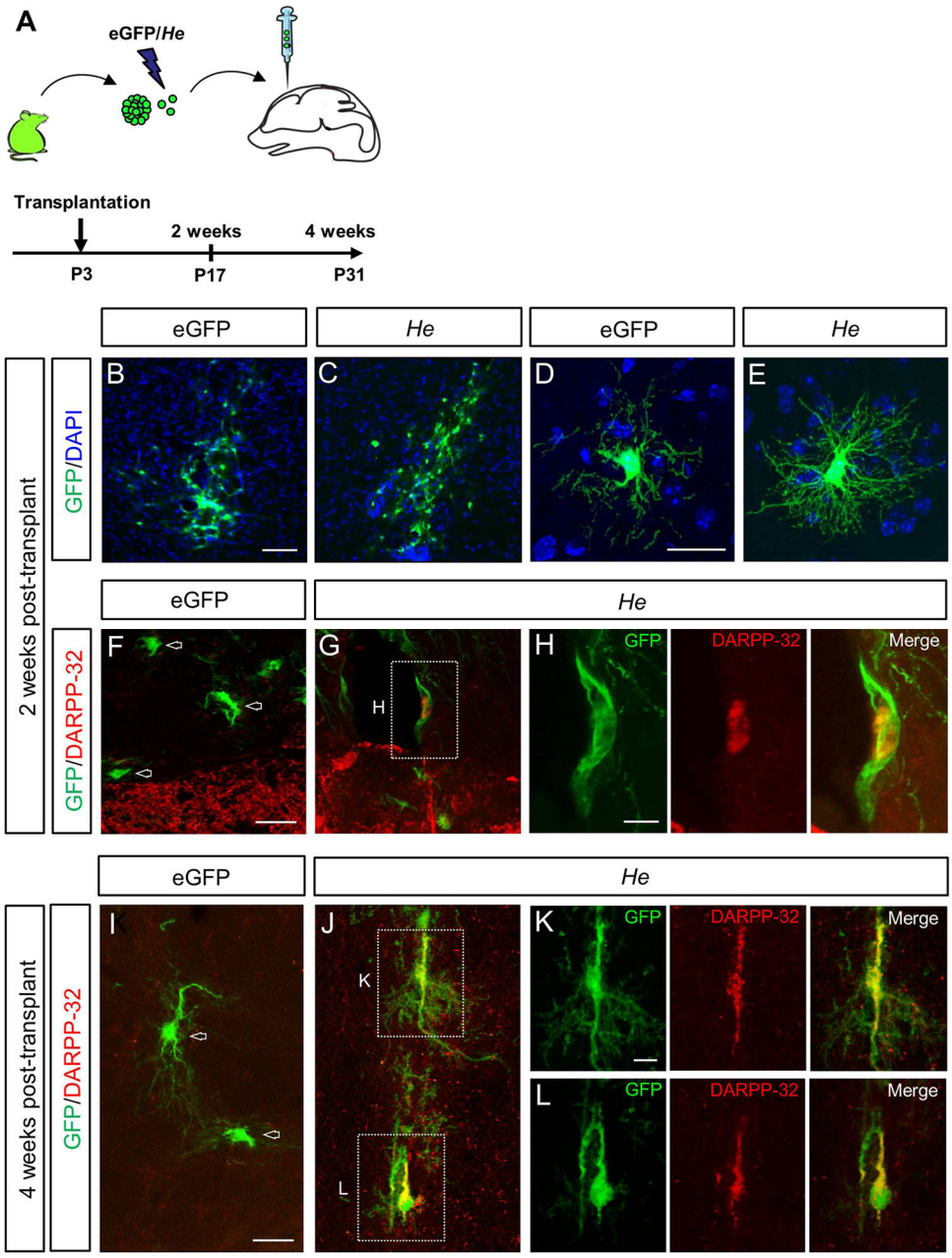

Fig. 7. *He* induces an MSN phenotype *in vivo*. (A) Schematic of the transplantation of eGFP and *He*-overexpressing NPCs into the mouse neonatal forebrain. (B-H) Representative images of forebrain coronal sections containing grafted cells 2 weeks post-transplantation, immunostained for GFP and DARPP-32. Compared with control cells (B,D), *He* overexpressing cells display more robust branching (C,E) and a few of them start to express DARPP-32 (G,H). (I-L) Representative images of grafted cells 4 weeks post-transplantation, labeled for GFP and DARPP-32. In contrast to control cells (I), several *He* overexpressing cells display DARPP-32 expression (J-L), indicative of the acquisition of a striatal MSN fate. Scale bars: 50 µm (B,C); 20 µm (D-G,I,J); 10 µm (H,K,L).

Previously published works and reviews suggest that striatal motor function is involved with habit formation (Yin and Knowlton, 2006) and procedural learning (Kreitzer, 2009), which fits with what we see in our $He^{-/-}$ mice. The striatum has been classically divided into dorsal and ventral areas, the dorsal being the most involved in motor behavior (Durieux et al., 2012). Accumulating evidence shows anatomical and functional differences in the striatum between the external DLS and the internal DMS (Durieux et al., 2012; Graybiel, 2008; Voorn et al., 2004). Interestingly, the DMS is involved in the initial stages of motor skill learning (Jueptner and Weiller, 1998; Luft and Buitrago, 2005), whereas the DLS is required for progressive skill automatization and habit learning (Miyachi et al., 2002; Yin et al., 2004). In addition, it has been shown that the loss of $D2R^+$ neurons in the DMS produces early motor learning impairment but the animals can improve their performances to reach control levels (Durieux et al., 2012). As $He^{-/-}$ mice show impairments in the acquisition of motor skills, it seems plausible that He is involved in the generation of a specific subpopulation of striatopallidal $D2R^+$ MSNs in the DMS. The cerebellum is also involved in fine-tuning the motor agility found in procedural skills. Cerebellar lesions or dysfunctions produce permanent deficits in motor tasks. However, diseased animals never perform motor tasks as well as their control or wt littermates (Sausbier et al., 2004; Stroobants et al., 2013; Vinueza Veloz et al., 2012). As $He^{-/-}$ mice show problems in the acquisition but not the execution of motor skills it seems that an association with cerebellar deficits is not likely.

Conclusion

In conclusion, our results demonstrate a novel mechanism for He in the development of striatopallidal MSNs of the DMS that controls motor skills learning. He exerts its main effects on the commitment

Development (2017) 144, 1566-1577 doi:10.1242/dev.138248

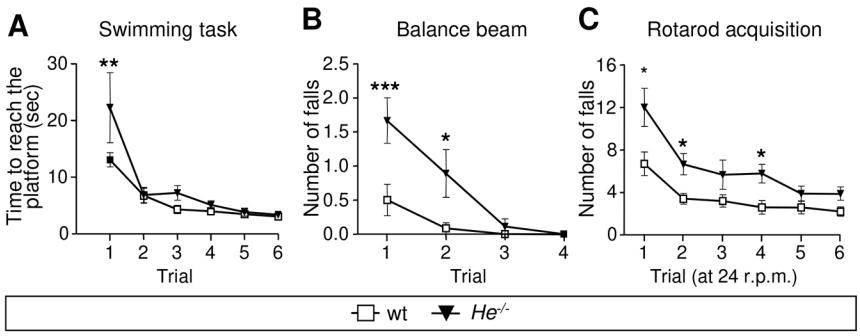

Fig. 8. The acquisition of new motor skills is impaired in *He*$^{-/-}$ mice. (A-C) Motor coordination and balance were analyzed in wt and *He*$^{-/-}$ mice by performing the simple swimming test (A), the balance beam (B) and the rotarod task (C). Values are expressed as mean±s.e.m. of 7-8 mice per condition. Data were analyzed by two-way ANOVA and Bonferroni's post-hoc test. **P*<0.05, ***P*<0.005, ****P*<0.001.

of NPCs to MSNs through the regulation of the G_1-S phase transition and arrests NPCs at G_1 phase to induce neuronal differentiation. The alterations of this mechanism observed in *He*$^{-/-}$ mice produce aberrant neurogenesis leading to the cell death of late-generated neurons.

MATERIALS AND METHODS

Animals

B6CBA wild-type (wt) mice (from Charles River Laboratories, Les Oncins, France), *He* knockout mice (*He*$^{-/-}$) (Cai et al., 2009), pCAGs-eGFP (Okabe et al., 1997), D1R-eGFP and D2R-eGFP generated by GENSAT (Gong et al., 2003) were used. For further details of mice strains and genotyping, see the supplementary Materials and Methods.

Birthdating, proliferation and tracking experiments *in vivo*

Birthdating experiments were performed as described elsewhere (Fig. 1B; Martín-Ibáñez et al., 2010). To study the generation of He$^+$ cells, injections of EdU (50 mg/kg) at E13.5 or E14.5, or BrdU at E16.5 into wt pregnant mice were performed and allowed to develop until E18.5, when embryos were processed for He and BrdU immunohistochemistry or EdU detection (Life Technologies) (Fig. S4A).

To analyze *in vivo* proliferation in the GZ, E14.5 pregnant mice received a single dose of EdU (50 mg/kg). The proliferation analysis of E16.5, P3 and P7 was performed by Ki67 immunohistochemistry.

In order to track the origin of dead cells in the MZ, a pulse of EdU (50 mg/kg) was performed at E18.5, and immunohistochemistry was performed at P3 against EdU and cleaved caspase 3 (Cell Signaling Technology), nestin, GFAP or NeuN (Fig. 5G).

To study whether the lack of *He* could alter the cells entering the S phase of the cell cycle, we performed *in vivo* experiments with *He*$^{-/-}$ and wt mice as previously described (Lange et al., 2009) (Fig. 4K).

For further details of these methods, see the supplementary Materials and Methods.

Production of viral particles and cell transduction

To overexpress *He*, NPCs were transduced with the pLV-*HE*-IRES-eGFP plasmid or the pLV-IRES-eGFP plasmid, which encode human *HE* and eGFP or eGFP alone, respectively. For further details of viral particle production, see the supplementary Materials and Methods.

Neurosphere assay

LGEs from E14.5 wt or *He*$^{-/-}$ mice were dissected out and mechanically disaggregated to culture as neurosphere and differentiate to neural cells as described previously (Martín-Ibáñez et al., 2010). For further details of neurosphere cultures, see the supplementary Materials and Methods.

Loss-of-function (LOF) experiments were performed with neurospheres derived from *He*$^{-/-}$ mice whereas gain-of-function (GOF) experiments were performed by overexpressing *He*. The number of neurons (β-III-tubulin$^+$) and astrocytes (GFAP$^+$) were analyzed after 6 days of differentiation.

Cell cycle analysis *in vitro*

Proliferation assays

BrdU incorporation assays were performed in wt and *He*$^{-/-}$ mice-derived neurospheres (LOF) and neurospheres overexpressing *He* (GOF) as described elsewhere (Urbán et al., 2010). The number of Ki67$^+$ cells was also analyzed in wt and *He*$^{-/-}$ mice-derived neurospheres (LOF) and neurospheres overexpressing *He* (GOF).

Cell cycle length

An accumulative exposure to 1 µM BrdU over 36 h was performed in wt and *He*$^{-/-}$ mice-derived neurospheres (LOF) and in neurospheres overexpressing *He* (GOF) after 2 DIV in proliferation. Cells were fixed at different time points after 1 µM BrdU exposure (1, 3, 6, 12, 24 and 36 h) and processed for BrdU immunocytochemistry. Following regression analysis as previously described by Takahashi et al. (1992, 1995), the length of the cell cycle and the length of the S phase were calculated for the NPCs.

S-phase analysis

To study the cells entering and exiting the S phase of the cell cycle, we performed *in vitro* experiments with neurospheres derived from *He*$^{-/-}$ and wt mice as described previously (Lange et al., 2009) (Fig. 3E-H).

G_2/M phase labeling

To study the combined length of the G_2/M phases, an accumulative exposure to 1 µM BrdU over 5 h was performed after 2 DIV in proliferation to analyze the mitotic BrdU labeling index as described previously (Takahashi et al., 1995).

Cell cycle index

We analyzed cell cycle index as the number of cells that incorporate BrdU but leave the cell cycle (i.e. abandoned the G_1-S-G_2/M phases and entered into G_0) as previously described (Urbán et al., 2010) (Fig. S13).

Discerning high and low Ki67-expressing cells

We detected cells expressing high and low levels of Ki67 using the automatic intensity detection of the Cell Profiler software.

For further details of cell cycle analyses, see the supplementary Materials and Methods.

Analysis of He-binding sites at the *Ccne1* promoter

We obtained and analyzed the Big Wig file deposited in Gene Expression Omnibus by Kim et al. (2015), and visualized it in the Integrative Genome Viewer with the files provided aligned to the Ensembl Mouse Genome. Details of database used can be found in the supplementary Materials and Methods.

Western blots

We performed western blot analyses for cyclin E and PCNA as described elsewhere (Canals et al., 2004) in wt and *He*$^{-/-}$ mice-derived neurospheres (LOF) and neurospheres overexpressing *He* (GOF). E2F1 and retinoblastoma (Rb) were detected in LOF experiments. For further details of western blot procedure, see the supplementary Materials and Methods.

In situ hybridization

To assess which striatal subpopulation of MSNs express *He*, we performed double *in situ* hybridization for ENK or tachykinin A (*Tac1*, a precursor of SP), the precursor of SP, and immunohistochemistry for He as described previously (Martín-Ibáñez et al., 2010). For further details of *in situ* procedures, see the supplementary Materials and Methods.

Development (2017) 144, 1566-1577 doi:10.1242/dev.138248

Immunolabeling

For histological preparations, embryonic or postnatal brains were removed at specific developmental stages and were frozen in dry ice-cooled methylbutane or cryoprotected depending on the procedure. Immunolabeling was performed according to the protocols described by Bosch et al. (2004) and Canals et al. (2004). For further details of the antibodies used and immunostaining procedures, see the supplementary Materials and Methods.

Measurement of volumes and *in vivo* cell counts

The volumes of certain brain regions were measured using ImageJ v1.33 as described previously (Canals et al., 2004). All cell counts [EdU and Ki67 for GZ proliferation; BrdU for birthdating experiments; cleaved caspase 3 for cell death; *Ctip2*, calbindin, DARPP-32, choline acetyl transferase (ChAT) and parvalbumin for striatal cell population] were performed blind to genotype. Unbiased stereological counts were performed for all striatal areas for each animal. DMS, DLS, VMS and VLS were specifically counted for DARPP-32-, ENK- and SP-positive cells.

The distribution of mitosis in $He^{-/-}$ and wt striatum at E16.5 was analyzed as described by Pilz et al. (2013) and counted using CAST software.

Automated quantification of branches, and neurite length was performed using Cell Profiler v2.8 software.

For further details of cell counts, see the supplementary Materials and Methods.

Q-PCR

Gene expression was evaluated by Q-PCR assays as previously described by Martín-Ibáñez et al. (2010). For further details of the probes used and PCR procedures, see the supplementary Materials and Methods.

Primary striatal culture and transfection

E14.5 fetal LGEs were dissected and cultured as previously described (Martín-Ibáñez et al., 2010). For *He* overexpression studies, cells were transfected with the MSCV-*He*-IRES-eGFP plasmid, or with the MSCV-IRES-eGFP plasmid as a control (Zhang et al., 2007). We counted the number of *He* or eGFP overexpressing cells that colocalized with calbindin, DARPP-32 or ENK. For further details of primary culture methods, see the supplementary Materials and Methods.

Cell transplants

Unilateral striatal injections of *He*-overexpressing cells were performed using a stereotaxic apparatus (Davis Kopf Instruments, Tujunga, CA, USA); coordinates (mm): AP, +2.3, L, +1.4 from lambda and DV, −1.8 from dura. For further details of cell transplants, see the supplementary Materials and Methods.

Mouse behavior

Swimming task

The mice were placed at the end of a transparent perspex extended swimming tank facing away from a visible escape platform at one end of the tank and the time taken to reach the platform was recorded.

Balance beam

Animals were allowed to walk along a horizontally placed beam of a long steel cylinder (50 cm) with 15 mm diameter. Latency to fall and number of falls were measured.

Rotarod

Acquisition of a motor coordination task was further evaluated on the rotarod apparatus (24 rpm). Latency to fall and the number of falls during 60 s was recorded.

For further details of mouse behavior analyses, see the supplementary Materials and Methods.

Statistical analysis

All results are expressed as the mean of independent experiments±s.e.m. Results were analyzed using Student's *t*-test or one-way or two-way ANOVA, followed by the Bonferroni post-hoc test.

Acknowledgements

The authors are very grateful to Dr Phil Sanders for critical reading of the manuscript, Dr David Vanneste for project managing and Ana López for technical assistance. We are also grateful to Dr Christopher A. Klug (Department of Microbiology, Division of Developmental and Clinical Immunology, University of Alabama at Birmingham, USA) for the MSCV-IRES-eGFP and MSCV-*He*-IRES-eGFP plasmids; Dr Pantelis Tsoulfas (University of Miami, FL, USA) for the pRRLsinPPT plasmids; and Dr Stephen T. Smale (Howard Hughes Medical Institute, Molecular Biology Institute, and Department of Microbiology and Immunology, UCLA School of Medicine, Los Angeles, CA, USA) for the anti-He antibody. The Rat-401 monoclonal anti-nestin antibody developed by S. Hockfield was obtained from the Development Studies Hybridoma Bank developed under the auspices of the NICHD and maintained by the Department of Biological Science, University of Iowa, Iowa City, IA, USA.

Competing interests

The authors declare no competing or financial interests.

Author contributions

R.M.-I. and M.P.: conceived this study, designed and performed experiments, analyzed data and prepared manuscript; A.G., A.M., I.G., L.M.-P., C.H., M.E. and G.G.-D.B.: performed experiments and analyzed data; M.J.E., C.V.-A., J.A., J.-A.G., S.C. and P.K.: contributed reagents/materials/analysis tools; J.M.C.: supervised and conceived this study, analyzed data and edited the manuscript.

Funding

This study was supported by grants from the Ministerio de Economía y Competitividad (BFU2010-19630 to C.V.-A.; SAF 2014-57160-R, to J. A.; SAF2015-66505-R to J.M.C.), and Instituto de Salud Carlos III-Subdirección General de Evaluación, and European Regional Development Fund (ERDF) [CIBERNED, to J. A and C.V.-A.; and RETICS (RD12/0019/0002; Red de Terapia Celular), to J.M.C.], Spain; Generalitat de Catalunya (2014SGR-968 to J.A.); Fundació la Marató de TV3 (20140130/1 to J.A.); and CHDI Foundation (A-7332 to J.M.C.). M.P. was a fellow from the Generalitat de Catalunya, Spain and E.C. was a fellow of the Ministerio de Economía y Competitividad, Spain. This work has been developed in the context of ADVANCE(CAT) with the support of ACCIÓ (Catalonia Trade & Investment; Generalitat de Catalunya) and the European Community under the Catalonian European Regional Development Fund operational program 2014-2020. Deposited in PMC for immediate release.

Supplementary information

Supplementary information available online at
http://dev.biologists.org/lookup/doi/10.1242/dev.138248.supplemental

References

Agoston, D. V., Szemes, M., Dobi, A., Palkovits, M., Georgopoulos, K., Gyorgy, A. and Ring, M. A. (2007). Ikaros is expressed in developing striatal neurons and involved in enkephalinergic differentiation. *J. Neurochem.* **102**, 1805-1816.

Alsiö, J. M., Tarchini, B., Cayouette, M. and Livesey, F. J. (2013). Ikaros promotes early-born neuronal fates in the cerebral cortex. *Proc. Natl. Acad. Sci. USA* **110**, E716-E725.

Alvarez-Buylla, A., García-Verdugo, J. M. and Tramontin, A. D. (2001). A unified hypothesis on the lineage of neural stem cells. *Nat. Rev. Neurosci.* **2**, 287-293.

Arai, Y., Pulvers, J. N., Haffner, C., Schilling, B., Nüsslein, I., Calegari, F. and Huttner, W. B. (2011). Neural stem and progenitor cells shorten S-phase on commitment to neuron production. *Nat. Commun.* **2**, 154.

Arlotta, P., Molyneaux, B. J., Jabaudon, D., Yoshida, Y. and Macklis, J. D. (2008). Ctip2 controls the differentiation of medium spiny neurons and the establishment of the cellular architecture of the striatum. *J. Neurosci.* **28**, 622-632.

Bohner, A. P., Akers, R. M. and McConnell, S. K. (1997). Induction of deep layer cortical neurons in vitro. *Development* **124**, 915-923.

Bosch, M., Pineda, J. R., Suñol, C., Petriz, J., Cattaneo, E., Alberch, J. and Canals, J. M. (2004). Induction of GABAergic phenotype in a neural stem cell line for transplantation in an excitotoxic model of Huntington's disease. *Exp. Neurol.* **190**, 42-58.

Brazel, C. Y., Romanko, M. J., Rothstein, R. P. and Levison, S. W. (2003). Roles of the mammalian subventricular zone in brain development. *Prog. Neurobiol.* **69**, 49-69.

Burek, M. J. and Oppenheim, R. W. (1996). Programmed cell death in the developing nervous system. *Brain Pathol.* **6**, 427-446.

Cai, Q., Dierich, A., Oulad-Abdelghani, M., Chan, S. and Kastner, P. (2009). Helios deficiency has minimal impact on T cell development and function. *J. Immunol.* **183**, 2303-2311.

Canals, J. M., Pineda, J. R., Torres-Peraza, J. F., Bosch, M., Martín-Ibañez, R., Muñoz, M. T., Mengod, G., Ernfors, P. and Alberch, J. (2004). Brain-derived neurotrophic factor regulates the onset and severity of motor dysfunction

Development (2017) 144, 1566-1577 doi:10.1242/dev.138248

associated with enkephalinergic neuronal degeneration in Huntington's disease. *J. Neurosci.* **24**, 7727-7739.

Cobb, B. S. and Smale, S. T. (2005). Ikaros-family proteins: in search of molecular functions during lymphocyte development. *Curr. Top. Microbiol. Immunol.* **290**, 29-47.

Dimou, L. and Götz, M. (2014). Glial cells as progenitors and stem cells: new roles in the healthy and diseased brain. *Physiol. Rev.* **94**, 709-737.

Durieux, P. F., Schiffmann, S. N. and de Kerchove d'Exaerde, A. (2012). Differential regulation of motor control and response to dopaminergic drugs by D1R and D2R neurons in distinct dorsal striatum subregions. *EMBO J.* **31**, 640-653.

Edlund, T. and Jessell, T. M. (1999). Progression from extrinsic to intrinsic signaling in cell fate specification: a view from the nervous system. *Cell* **96**, 211-224.

Ehrman, L. A., Mu, X., Waclaw, R. R., Yoshida, Y., Vorhees, C. V., Klein, W. H. and Campbell, K. (2013). The LIM homeobox gene Isl1 is required for the correct development of the striatonigral pathway in the mouse. *Proc. Natl. Acad. Sci. USA* **110**, E4026-E4035.

Eisenstat, D. D., Liu, J. K., Mione, M., Zhong, W., Yu, G., Anderson, S. A., Ghattas, I., Puelles, L. and Rubenstein, J. L. (1999). DLX-1, DLX-2, and DLX-5 expression define distinct stages of basal forebrain differentiation. *J. Comp. Neurol.* **414**, 217-237.

Ericson, J., Morton, S., Kawakami, A., Roelink, H. and Jessell, T. M. (1996). Two critical periods of Sonic Hedgehog signaling required for the specification of motor neuron identity. *Cell* **87**, 661-673.

Flames, N., Pla, R., Gelman, D. M., Rubenstein, J. L. R., Puelles, L. and Marín, O. (2007). Delineation of multiple subpallial progenitor domains by the combinatorial expression of transcriptional codes. *J. Neurosci.* **27**, 9682-9695.

Garcia-Dominguez, M., Poquet, C., Garel, S. and Charnay, P. (2003). Ebf gene function is required for coupling neuronal differentiation and cell cycle exit. *Development* **130**, 6013-6025.

Garel, S., Marín, F., Grosschedl, R. and Charnay, P. (1999). Ebf1 controls early cell differentiation in the embryonic striatum. *Development* **126**, 5285-5294.

Georgopoulos, K. (2002). Haematopoietic cell-fate decisions, chromatin regulation and ikaros. *Nat. Rev. Immunol.* **2**, 162-174.

Gerfen, C. R. (1992). The neostriatal mosaic: multiple levels of compartmental organization. *Trends Neurosci.* **15**, 133-139.

Gong, S., Zheng, C., Doughty, M. L., Losos, K., Didkovsky, N., Schambra, U. B., Nowak, N. J., Joyner, A., Leblanc, G., Hatten, M. E. et al. (2003). A gene expression atlas of the central nervous system based on bacterial artificial chromosomes. *Nature* **425**, 917-925.

Götz, M. and Barde, Y.-A. (2005). Radial glial cells defined and major intermediates between embryonic stem cells and CNS neurons. *Neuron* **46**, 369-372.

Gould, E., Reeves, A. J., Graziano, M. S. and Gross, C. G. (1999). Neurogenesis in the neocortex of adult primates. *Science* **286**, 548-552.

Graybiel, A. M. (2008). Habits, rituals, and the evaluative brain. *Annu. Rev. Neurosci.* **31**, 359-387.

Hahm, K., Cobb, B. S., McCarty, A. S., Brown, K. E., Klug, C. A., Lee, R., Akashi, K., Weissman, I. L., Fisher, A. G. and Smale, S. T. (1998). Helios, a T cell-restricted Ikaros family member that quantitatively associates with Ikaros at centromeric heterochromatin. *Genes Dev.* **12**, 782-796.

Harbour, J. W. (2000). The Rb/E2F pathway: expanding roles and emerging paradigms. *Genes Dev.* **14**, 2393-2409.

Hardwick, L. J. A. and Philpott, A. (2014). Nervous decision-making: to divide or differentiate. *Trends Genet.* **30**, 254-261.

John, L. B., Yoong, S. and Ward, A. C. (2009). Evolution of the Ikaros gene family: implications for the origins of adaptive immunity. *J. Immunol.* **182**, 4792-4799.

Jueptner, M. and Weiller, C. (1998). A review of differences between basal ganglia and cerebellar control of movements as revealed by functional imaging studies. *Brain* **121**, 1437-1449.

Kanthan, R., Fried, I., Rueckl, T., Senger, J.-L. and Kanthan, S. C. (2010). Expression of cell cycle proteins in male breast carcinoma. *World J. Surg. Oncol.* **8**, 10.

Kim, H.-J., Hida, H., Jung, C.-G., Miura, Y. and Nishino, H. (2006). Treatment with deferoxamine increases neurons from neural stem/progenitor cells. *Brain Res.* **1092**, 1-15.

Kim, H.-J., Barnitz, R. A., Kreslavsky, T., Brown, F. D., Moffett, H., Lemieux, M. E., Kaygusuz, Y., Meissner, T., Holderried, T. A. W., Chan, S. et al. (2015). Stable inhibitory activity of regulatory T cells requires the transcription factor Helios. *Science* **350**, 334-339.

Kreitzer, A. C. (2009). Physiology and pharmacology of striatal neurons. *Annu. Rev. Neurosci.* **32**, 127-147.

Kristiansen, M. and Ham, J. (2014). Programmed cell death during neuronal development: the sympathetic neuron model. *Cell Death Differ.* **21**, 1025-1035.

Lacomme, M., Liaubet, L., Pituello, F. and Bel-Vialar, S. (2012). NEUROG2 drives cell cycle exit of neuronal precursors by specifically repressing a subset of cyclins acting at the G1 and S phases of the cell cycle. *Mol. Cell. Biol.* **32**, 2596-2607.

Lange, C., Huttner, W. B. and Calegari, F. (2009). Cdk4/cyclinD1 overexpression in neural stem cells shortens G1, delays neurogenesis, and promotes the generation and expansion of basal progenitors. *Cell Stem Cell* **5**, 320-331.

Leng, X., Connell-Crowley, L., Goodrich, D. and Harper, J. W. (1997). S-phase entry upon ectopic expression of G1 cyclin-dependent kinases in the absence of retinoblastoma protein phosphorylation. *Curr. Biol.* **7**, 709-712.

Lobo, M. K., Karsten, S. L., Gray, M., Geschwind, D. H. and Yang, X. W. (2006). FACS-array profiling of striatal projection neuron subtypes in juvenile and adult mouse brains. *Nat. Neurosci.* **9**, 443-452.

Lobo, M. K., Yeh, C. and Yang, X. W. (2008). Pivotal role of early B-cell factor 1 in development of striatonigral medium spiny neurons in the matrix compartment. *J. Neurosci. Res.* **86**, 2134-2146.

Lopez, F., Belloc, F., Lacombe, F., Dumain, P., Reiffers, J., Bernard, P. and Boisseau, M. R. (1991). Modalities of synthesis of Ki67 antigen during the stimulation of lymphocytes. *Cytometry* **12**, 42-49.

Lu, K.-M., Evans, S. M., Hirano, S. and Liu, F.-C. (2014). Dual role for Islet-1 in promoting striatonigral and repressing striatopallidal genetic programs to specify striatonigral cell identity. *Proc. Natl. Acad. Sci. USA* **111**, E168-E177.

Luft, A. R. and Buitrago, M. M. (2005). Stages of motor skill learning. *Mol. Neurobiol.* **32**, 205-216.

Lukas, J., Herzinger, T., Hansen, K., Moroni, M. C., Resnitzky, D., Helin, K., Reed, S. I. and Bartek, J. (1997). Cyclin E-induced S phase without activation of the pRb/E2F pathway. *Genes Dev.* **11**, 1479-1492.

Martín-Ibáñez, R., Crespo, E., Urbán, N., Sergent-Tanguy, S., Herranz, C., Jaumot, M., Valiente, M., Long, J. E., Pineda, J. R., Andreu, C. et al. (2010). Ikaros-1 couples cell cycle arrest of late striatal precursors with neurogenesis of enkephalinergic neurons. *J. Comp. Neurol.* **518**, 329-351.

Martín-Ibáñez, R., Crespo, E., Esgleas, M., Urban, N., Wang, B., Waclaw, R., Georgopoulos, K., Martínez, S., Campbell, K., Vicario-Abejón, C. et al. (2012). Helios transcription factor expression depends on Gsx2 and Dlx1&2 function in developing striatal matrix neurons. *Stem Cells Dev.* **21**, 2239-2251.

Mason, H. A., Rakowiecki, S. M., Raftopoulou, M., Nery, S., Huang, Y., Gridley, T. and Fishell, G. (2005). Notch signaling coordinates the patterning of striatal compartments. *Development* **132**, 4247-4258.

McConnell, S. K. and Kaznowski, C. E. (1991). Cell cycle dependence of laminar determination in developing neocortex. *Science* **254**, 282-285.

Merkle, F. T. and Alvarez-Buylla, A. (2006). Neural stem cells in mammalian development. *Curr. Opin. Cell Biol.* **18**, 704-709.

Mérot, Y., Rétaux, S. and Heng, J. I.-T. (2009). Molecular mechanisms of projection neuron production and maturation in the developing cerebral cortex. *Semin. Cell Dev. Biol.* **20**, 726-734.

Misumi, S., Kim, T.-S., Jung, C.-G., Masuda, T., Urakawa, S., Isobe, Y., Furuyama, F., Nishino, H. and Hida, H. (2008). Enhanced neurogenesis from neural progenitor cells with G1/S-phase cell cycle arrest is mediated by transforming growth factor beta1. *Eur. J. Neurosci.* **28**, 1049-1059.

Miyachi, S., Hikosaka, O. and Lu, X. (2002). Differential activation of monkey striatal neurons in the early and late stages of procedural learning. *Exp. Brain Res.* **146**, 122-126.

Ninkovic, J. and Götz, M. (2013). Fate specification in the adult brain – lessons for eliciting neurogenesis from glial cells. *BioEssays* **35**, 242-252.

Ohtani, K., DeGregori, J. and Nevins, J. R. (1995). Regulation of the cyclin E gene by transcription factor E2F1. *Proc. Natl. Acad. Sci. USA* **92**, 12146-12150.

Ohtsubo, M. and Roberts, J. M. (1993). Cyclin-dependent regulation of G1 in mammalian fibroblasts. *Science* **259**, 1908-1912.

Ohtsubo, M., Theodoras, A. M., Schumacher, J., Roberts, J. M. and Pagano, M. (1995). Human cyclin E, a nuclear protein essential for the G1-to-S phase transition. *Mol. Cell. Biol.* **15**, 2612-2624.

Okabe, M., Ikawa, M., Kominami, K., Nakanishi, T. and Nishimune, Y. (1997). 'Green mice' as a source of ubiquitous green cells. *FEBS Lett.* **407**, 313-319.

Pilaz, L.-J., Patti, D., Marcy, G., Ollier, E., Pfister, S., Douglas, R. J., Betizeau, M., Gautier, E., Cortay, V., Doerflinger, N. et al. (2009). Forced G1-phase reduction alters mode of division, neuron number, and laminar phenotype in the cerebral cortex. *Proc. Natl. Acad. Sci. USA* **106**, 21924-21929.

Pilz, G.-A., Shitamukai, A., Reillo, I., Pacary, E., Schwausch, J., Stahl, R., Ninkovic, J., Snippert, H. J., Clevers, H., Godinho, L. et al. (2013). Amplification of progenitors in the mammalian telencephalon includes a new radial glial cell type. *Nat. Commun.* **4**, 2125.

Rallu, M., Corbin, J. G. and Fishell, G. (2002). Parsing the prosencephalon. *Nat. Rev. Neurosci.* **3**, 943-951.

Rebollo, A. and Schmitt, C. (2003). Ikaros, Aiolos and Helios: transcription regulators and lymphoid malignancies. *Immunol. Cell Biol.* **81**, 171-175.

Resnitzky, D., Gossen, M., Bujard, H. and Reed, S. I. (1994). Acceleration of the G1/S phase transition by expression of cyclins D1 and E with an inducible system. *Mol. Cell. Biol.* **14**, 1669-1679.

Sausbier, M., Hu, H., Arntz, C., Feil, S., Kamm, S., Adelsberger, H., Sausbier, U., Sailer, C. A., Feil, R., Hofmann, F. et al. (2004). Cerebellar ataxia and Purkinje cell dysfunction caused by $Ca2^{+}$-activated K^{+} channel deficiency. *Proc. Natl. Acad. Sci. USA* **101**, 9474-9478.

Scholzen, T. and Gerdes, J. (2000). The Ki-67 protein: from the known and the unknown. *J. Cell. Physiol.* **182**, 311-322.

Stroobants, S., Gantois, I., Pooters, T. and D'Hooge, R. (2013). Increased gait variability in mice with small cerebellar cortex lesions and normal rotarod performance. *Behav. Brain Res.* **241**, 32-37.

Development (2017) 144, 1566-1577 doi:10.1242/dev.138248

Takahashi, T., Nowakowski, R. S. and Caviness, V. S. (1992). BUdR as an S-phase marker for quantitative studies of cytokinetic behaviour in the murine cerebral ventricular zone. *J. Neurocytol.* **21**, 185-197.

Takahashi, T., Nowakowski, R. S. and Caviness, V. S. (1995). The cell cycle of the pseudostratified ventricular epithelium of the embryonic murine cerebral wall. *J. Neurosci.* **15**, 6046-6057.

Tanabe, Y., William, C. and Jessell, T. M. (1998). Specification of motor neuron identity by the MNR2 homeodomain protein. *Cell* **95**, 67-80.

Turrero García, M., Chang, Y., Arai, Y. and Huttner, W. B. (2015). S-phase duration is the main target of cell cycle regulation in neural progenitors of developing ferret neocortex. *J. Comp. Neurol.* **524**, 456-470.

Urbán, N., Martín-Ibáñez, R., Herranz, C., Esgleas, M., Crespo, E., Pardo, M., Crespo-Enríquez, I., Méndez-Gómez, H. R., Waclaw, R., Chatzi, C. et al. (2010). Nolz1 promotes striatal neurogenesis through the regulation of retinoic acid signaling. *Neural Dev.* **5**, 21.

Vinueza Veloz, M. F., Buijsen, R. A. M., Willemsen, R., Cupido, A., Bosman, L. W. J., Koekkoek, S. K. E., Potters, J. W., Oostra, B. A. and De Zeeuw, C. I. (2012). The effect of an mGluR5 inhibitor on procedural memory and avoidance discrimination impairments in Fmr1 KO mice. *Genes. Brain. Behav.* **11**, 325-331.

Voorn, P., Vanderschuren, L. J. M. J., Groenewegen, H. J., Robbins, T. W. and Pennartz, C. M. A. (2004). Putting a spin on the dorsal-ventral divide of the striatum. *Trends Neurosci.* **27**, 468-474.

Waclaw, R. R., Wang, B., Pei, Z., Ehrman, L. A. and Campbell, K. (2009). Distinct temporal requirements for the homeobox gene Gsx2 in specifying striatal and olfactory bulb neuronal fates. *Neuron* **63**, 451-465.

Yin, H. H. and Knowlton, B. J. (2006). The role of the basal ganglia in habit formation. *Nat. Rev. Neurosci.* **7**, 464-476.

Yin, H. H., Knowlton, B. J. and Balleine, B. W. (2004). Lesions of dorsolateral striatum preserve outcome expectancy but disrupt habit formation in instrumental learning. *Eur. J. Neurosci.* **19**, 181-189.

Yoshida, T. and Georgopoulos, K. (2014). Ikaros fingers on lymphocyte differentiation. *Int. J. Hematol.* **100**, 220-229.

Yun, K., Fischman, S., Johnson, J., Hrabe de Angelis, M., Weinmaster, G. and Rubenstein, J. L. R. (2002). Modulation of the notch signaling by Mash1 and Dlx1/2 regulates sequential specification and differentiation of progenitor cell types in the subcortical telencephalon. *Development* **129**, 5029-5040.

Zhang, Z., Swindle, C. S., Bates, J. T., Ko, R., Cotta, C. V. and Klug, C. A. (2007). Expression of a non-DNA-binding isoform of Helios induces T-cell lymphoma in mice. *Blood* **109**, 2190-2197.

SUPPLEMENTARY MATERIALS AND METHODS

Animals

Mice were maintained in standard conditions with food and water ad libitum. All animal procedures were approved by local committees, in accordance with the European Communities Council Directive (86/609/EU). B6CBA wild-type (wt) mice (from Charles River Laboratories, Les Oncins, France), *He* knockout mice ($He^{-/-}$) (Cai et al., 2009), pCAGs-eGFP [enhanced green fluorescent protein under the control of a chicken beta-actin promoter and cytomegalovirus enhancer] (Okabe et al., 1997), D1R-eGFP [enhanced green fluorescent protein under the control of D1R] and D2R-eGFP [enhanced green fluorescent protein under the control of D2R] generated by GENSAT (Bertran-Gonzalez et al., 2008; Gong et al., 2003) were used. These strains were maintained by backcrossing to C57BL/6 mice. $He^{-/-}$ mice show high perinatal death as it is described elsewhere (Cai et al., 2009). Genotypes were determined by PCR as described elsewhere (Cai et al., 2009). The day of pregnancy, determined by the first detection of a vaginal sperm plug in daily inspection, was considered embryonic day (E)0.5.

Birth dating, proliferation and tracking experiments *in vivo*

To study neurogenesis in wt and $He^{-/-}$ mice, birth dating experiments were performed as described elsewhere (Martín-Ibáñez et al., 2010). Briefly, pregnant mice were injected intra-peritoneally with bromo deoxyuridine (BrdU; 50 mg/kg; Sigma Chemical Co., St. Louis, MO). BrdU was administered at E12.5, E14.5, and E16.5, and the embryos were subsequently allowed to develop until E18.5, at which point the dams were terminally anesthetized and the embryos were removed and processed for BrdU immunohistochemistry. For a representative scheme, see Fig.1B.

Development • Supplementary information

To analyze proliferation in the GZ *in vivo*, E14.5 pregnant mice received a single dose of ethynyl deoxyuridine (EdU; 50 mg/Kg; C10420, Click-iT® EdU Alexa Fluor® 488 Flow Cytometry Assay Kit; Life Technologies S.A., Alcobendas, Madrid). Thirty minutes later they were terminally anesthetized, and the embryos were processed for EdU detection (according to the manufacturer's instructions). The proliferation analysis of other stages such E16.5, P3 and P7 was performed by Ki67 immunohistochemistry as explained below. Although we also performed Ki67 staining at E14.5, it was not reliably detectable at this stage. For this reason we showed the co-labeling between Ki67 and *He* at E16.5.

To study the generation of *He* positive cells, injections of EdU at E13.5 or E14.5, and BrdU at E16.5 into wt pregnant mice were performed and the embryos were allowed to develop until E18.5, at which point the dams were terminally anesthetized and the embryos were removed and processed for *He* and BrdU immunohistochemistry or EdU detection (Life Technologies S.A.). For a representative scheme, see Fig.S4A.

In order to track the origin of dead cells in the MZ, a pulse of EdU was performed at E18.5 in pregnant mice, and the pups were allowed to develop until P3, at which point the brains were recovered and immunohistochemistry was performed against Cleaved caspase 3 (Cell Signaling Technology, Inc. Danvers MA), Nestin GFAP, or NeuN and EdU. For a representative scheme, see Fig.5G.

To study if the lack of Helios could alter the cells entering or exiting the S-phase of the cell cycle, we performed *in vivo* experiments with $He^{-/-}$ and wt mice as previously described (Lange et al., 2009). Briefly, an initial injection of BrdU (50 mg/kg) was performed in $He^{-/-}$ pregnant females at E14.5. After 45 minutes, a second injection of EdU (50 mg/Kg) was performed. Finally, 45 minutes later, the female was sacrificed and the E14.5 embryos were collected and processed to perform immunohistochemistry.

Development • Supplementary information

Double staining for BrdU and EdU permitted the identification of two different cell populations: first population - double labeled cells for EdU and BrdU with a punctate staining corresponding to cells entering S phase; second population - cells single labeled for BrdU, corresponding to cells leaving S phase. For a representative scheme, see Fig.4E.

Production of viral particles and cell transduction

To over-express *He*, NSCs were transduced with the pLV-*He*-IRES-eGFP plasmid or the pLV-IRES-eGFP plasmid which encode human *He* and enhanced green fluorescent protein (eGFP) or eGFP alone, respectively. The pLV-IRES-eGFP plasmid was generated as described elsewhere (Urbán et al., 2010). Briefly, MCS-IRES-eGFP was cloned from the pRV-IRES-eGFP plasmid (Genetrix SL, Tres Cantos, Madrid, Spain) using the *Bam*HI and the *Sal*I restriction sites into the pRRLsinPPT plasmid (pRRL) constructed by the Miami Project to Cure Paralysis Viral Vector Core Lab based on the lentiviral transducing plasmid developed by Naldini et al. (Naldini et al., 1996). To construct the pLV-*He*-IRES-EGFP, the human *He* gene from the SPORT6-*He* plasmid (Life Technologies S.A.) was cloned into the *Bam*HI and *Xho*I sites of pLV-IRES-eGFP.

For lentivirus production 293T cells were plated at a density of approximately 6 x 10^4 cells per cm^2. The following day, cells were transfected with a three-plasmid system (the pLV-IRES-eGFP or pLV-*He*-IRES-eGFP plasmids, the plasmid that expresses HIV-1 *gag* and *pol* genes, and the plasmid that expresses vesicular stomatitis virus G) using the calcium phosphate/DNA co- precipitation method. Cells were transfected for 7h and subsequently the medium was removed and replaced with fresh medium. The supernatant from vector-producing 293T cells was collected every 22 h over 3 days. The supernatant was then passed through a 0.45-µm-pore-size filter to remove producer cells

Development • Supplementary information

and subjected to 2 centrifugations at 4°C and 25000 x *g* for 120 min to concentrate the virus. The virus-containing pellet was dissolved in 1% BSA. To determine the viral titer, a total of 2 x 10^5 293T cells were inoculated with serial dilutions of concentrated lentivirus. Forty-eight hours after infection, eGFP titers (international units per ml) were determined using a fluorescence-activated cell scanner (FACS).

Neurosphere assay

LGEs from E14.5 wt or *He*$^{-/-}$ mice were dissected out and mechanically disaggregated as described previously (Martín-Ibáñez et al., 2010). Briefly, LGE-derived neurosphere cultures were obtained by seeding 50000 cells/cm^2 in basal medium [Dulbecco's Modified Eagle's Medium (DMEM; Sigma Chemical Co.):F12 (Life Technologies S.A.) (1:1), 0.3% glucose (Sigma Chemical Co.), 0.3 mg/ml glutamine (Life Technologies S.A.), 5 mM HEPES (Life Technologies S.A.), 100 U/ml penicillin, 100 mg/ml streptomycin (Life Technologies S.A.), 4 µg/ml heparin (Sigma Chemical Co.), 4 mg/ml BSA (Sigma Chemical Co.), 1X N2 supplement (Life Technologies S.A.)], supplemented with 20 ng/ml fibroblast growth factor (FGF; Sigma Chemical Co.) and 10 ng/ml epidermal growth factor (EGF; Life Technologies S.A.). Every 5 days neurospheres were collected, dissociated by pipetting approximately 40 times with a P100 micropipette, and plated down in fresh media at a density of 10000 cells/cm^2. All experiments were performed with at least 3-4 independent neurosphere cultures between passages 4-7.

For differentiation studies, the day after plating cells were collected and allowed to attach to coverslips pre-coated with Matrigel^{TM} (Growth Factor Reduced Matrigel Matrix; BD Biosciences, San Agustín de Guadalix, Madrid) in MD1 medium containing: basal medium supplemented with 20 ng/ml FGF (Sigma Chemical Co.). NSCs were differentiated in this medium for three days and then the culture medium

Development • Supplementary information

was changed to MD2 containing basal medium supplemented with 2% fetal bovine serum (FBS; Life Technologies S.A.) for 3 additional days. Cells were fixed with 4% paraformaldehyde (PFA; Merck Biosciences Ltd., Nottingham, UK) solution in phosphate-buffered saline, pH 7.4 (PBS) and processed for immunocytochemistry analyses. Loss of function (LOF) experiments were performed with neurospheres derived from *He*$^{-/-}$ mice and compared to the control neurospheres derived from wt mice. Gain of function (GOF) experiments were performed by over-expressing *He* via the transduction of neurospheres the first day after plating with pLV-*He*-IRES-eGFP lentivirus or the control pLV-IRES-eGFP. The number of neurons (positive for β-III-tubulin) and astrocytes (positive for GFAP) were analyzed after 6 days in differentiation in LOF and GOF experiments. Results are expressed as the percentage of cells positive for each marker. All experiments were performed with at least 3-4 independent neurosphere cultures between passages 4-7.

Cell Cycle analysis *in vitro*

Proliferation assays

BrdU incorporation assays were performed in wt and *He*$^{-/-}$ mice derived neurospheres (for LOF experiments) and neurospheres over-expressing pLV-*He*-IRES-eGFP or pLV-IRES-eGFP (for GOF experiments) as described elsewhere (Urbán et al., 2010). LOF experiments were performed by seeding 25000 cells in a P24 well plate in proliferative conditions and after three days the cells were treated with 1μM BrdU (Sigma Chemical Co.) for 20 minutes, collected and incubated for 10 minutes in P24 well plates containing glass coverslips pre-coated with Matrigel^{TM} (BD Biosciences) to enhance attachment of cells to the surface. Immediately after incubation, cells were fixed with 4% PFA solution. Once fixed, neurosphere preparations were incubated for 30 min in 2N HCl followed by treatment with Sodium Borate 0.1M for 20 minutes and processed

Development • Supplementary information

for immunocytochemistry against BrdU. For GOF experiments, 25000 cells were seeded in a P24 well plate in proliferative conditions and infected with pLV-*He*-IRES-eGFP or the control pLV-IRES-eGFP lentivirus using a multiplicity of infection (MOI) of 2.5. After cell transduction, the BrdU assay was performed following the protocol described for wt and $He^{-/-}$ neurospheres. The percentage of cells incorporating BrdU was quantified.

The same cultures were processed for immunocytochemistry against Ki67 to further analyze the percentage of proliferating cells in LOF and GOF experiments. These experiments were performed with at least 3-4 independent neurosphere cultures between passages 4-7.

Cell cycle length

An accumulative exposure to 1µM BrdU during 36 hours was performed in wt and $He^{-/-}$ mice derived neurospheres (LOF) and in neurospheres over-expressing pLV-*He*-IRES-eGFP or pLV-IRES-eGFP (GOF) after 2DIV in proliferation. At different time points after 1µM BrdU exposure (1, 3, 6, 12, 24 and 36 hours), cells were collected and incubated for 10 minutes in P24 well plates containing glass coverslips pre-coated with Matrigel™ (BD Biosciences) to enhance attachment of cells to the surface. Immediately after incubation cells were fixed with 4% PFA solution and processed for BrdU immunocytochemistry. Analysis of the percentage of BrdU positive cells over time gives rise to a curve that at a certain time point reaches a plateau phase, where all the cells in proliferation are labeled with BrdU. Following a regression analysis as previously described by Takahashi et al (Takahashi et al., 1992; Takahashi et al., 1995), the length of the cell cycle and the length of the S phase were calculated for the NPCs in the presence and absence of *He*. These experiments were performed with at least 3-4 independent neurosphere cultures between passages 4-7.

Development • Supplementary information

S-phase analysis

To study the cells entering and exiting the S-phase of the cell cycle, we performed *in vitro* experiments with neurospheres derived from *He*$^{-/-}$ and wt mice as previously described (Lange et al., 2009). Briefly, an initial pulse of 1µM BrdU was performed in a culture of proliferating neurospheres growing for 2 days in vitro (2DIV). Then, after 45 minutes a second pulse of 1µM EdU was performed. After a further 45 minutes cells were collected and incubated for 10 minutes in P24 well plates containing glass coverslips pre-coated with Matrigel™ (BD Biosciences) to enhance attachment of cells to the surface. Immediately after incubation cells were fixed with 4% PFA solution and processed for immunocytochemistry. The percentage of double for EdU and BrdU with a punctate staining corresponding to cells entering S phase or single labeled cells for BrdU corresponding to cells leaving S phase were quantified for wt and *He*$^{-/-}$ mice derived neurospheres (see representative scheme in Fig.4E). These experiments were performed with at least 3-4 independent neurosphere cultures between passages 4-7.

G_2/M phase labeling

To study the combined length of the G_2/M phases, an accumulative exposure to 1µM BrdU over 5 hours was performed in wt and *He*$^{-/-}$ mice derived neurospheres (LOF) and neurospheres over-expressing pLV-*He*-IRES-eGFP or pLV-IRES-eGFP (GOF) after 2 DIV in proliferation. At different time points (30 minutes, 1, 2, 3, 4 and 5 hours), cells were collected and incubated for 10 minutes in P24 well plates containing glass coverslips pre-coated with Matrigel™ (BD Biosciences) to enhance attachment of cells to the surface. Immediately after incubation cells were fixed with 4% PFA solution and processed for BrdU immunocytochemistry. Analysis of the mitotic BrdU labeling index was performed as described previously (Takahashi et al., 1995). The percentage of mitotic cells positive for BrdU was counted at each time point for both cell cultures.

Development • Supplementary information

The time required to label all mitotic figures with BrdU is considered as the length of the combined G_2/M phases (Takahashi et al., 1995). These experiments were performed with at least 3-4 independent neurosphere cultures between passages 4-7.

Cell cycle index

We analyzed cell cycle index as the number of cells that retain BrdU but leave the cell cycle (abandoned the G_1-S-G_2/M phases and entered into G_0) as previously described (Urbán et al., 2010). These experiments were performed in wt and *He*$^{-/-}$ mice derived neurospheres (for LOF experiments) and neurospheres over-expressing pLV-*He*-IRES-eGFP or pLV-IRES-eGFP (for GOF experiments). Briefly, 25000 cells were seeded in a P24 well plate in proliferative conditions and after two days the cells were treated for 24 hours with 1µM BrdU (Sigma Chemical Co.), collected and incubated for 10 minutes in P24 well plates containing glass coverslips pre-coated with Matrigel™ (BD Biosciences) to enhance attachment of cells to the surface. Immediately after incubation, cells were fixed with 4% PFA solution. Double immunohistochemistry against BrdU and Ki67 was performed, and the combination of these markers allowed the quantification of the fraction of cell cycle index (cells that abandoned cell cycle and entered into G_0, single labeled with BrdU) or cells still in proliferation (double labeled with BrdU and Ki67). For a representative scheme see Fig.S13A. These experiments were performed with at least 3-4 independent neurosphere cultures between passages 4-7.

Discerning high and low Ki expressing cells

We detected high and low expressing KI67 cells with the automatic intensity detection of the Cell Profiler software. Briefly the grayscale 16 bit images from each color channel were included in an automated pipeline that identified objects within the range of typical diameter of 15 to 45 pixels (IdentifyPrimaryObjects module), then its shape

Development • Supplementary information

and intensity was measured (MeasureObjectIntensity module), we visualized the results in an histogram of intensities distribution where two populations were easily separated. We determined the appropriate threshold (0.03 AU) to distinguish between high and low intensity objects.

Analysis of the He binding sites at the *Ccne* promoter

In order to corroborate the binding of Helios with promoter regions detected on the Cyclin E gene (Ccne1) we obtained the Big Wig file from the GEO repository of the article by (Kim et al., 2015) (GEO Series GSE72997), and visualized it in the Integrative Genome Viewer with the files provided aligned to the Ensembl Mouse Genome [version mm9; http://www.ensembl.org/Mus_musculus/Info/Index; European Bioinformatics Institute (EMBI-EBI) and the Wellcome Trust Sanger Institute (WTSI); Wellcome Trust Genome Campus; Hinxton, UK].

Western blots

We analyzed cell cycle protein levels in LOF and GOF *in vitro* and *in vivo*: neurospheres overexpressing *He* or eGFP, $He^{-/-}$ and wt neurospheres, and $He^{-/-}$ or wt E14.5 LGEs. Samples were prepared and processed for western blot as described elsewhere (Canals et al., 2004). Briefly, samples were homogenated by BioRuptor Sonicator (Diagenode) in 100 µl assay buffer (50 mM Tris-HCl, pH 7.5; 150 mM NaCl; 10% glycerol; 10 mM EGTA, 1% Triton X-100; 100mM NaF; 5µM $ZnCl_2$; 1 µg/ml Leupeptin; 8 µl/ml PMSF; 1 µg/ml Aprotinin and 2.5 µl/ml Orthovanadate). Between fifteen and twenty micrograms of the homogenates were loaded in a 10% SDS-PAGE (sodium dodecyl sulfate-polyacrylamide gel electrophoresis) and transferred to Immobilon-P membranes (Milipore, Bedford, MA). Blots were incubated overnight at 4°C with 1:750 of anti-CyclinE antibody (M-20, rabbit polyclonal; Santa Cruz

Development • Supplementary information

Biotechnology Inc), 1:750 of anti-E2F1 antibody (Sc-251, Santa Cruz Biotechnology Inc), 1:750 of anti-retinoblastoma (Rb) antibody (C15, Santa Cruz Biotechnology Inc) or anti-PCNA (PC-10, Santa Cruz Biotechnology Inc.), and after several washes in Tris-buffered saline containing 0.1% v/v Tween-20 (TBS-T), membranes were incubated with an HRP-conjugated anti-rabbit IgG (1:1000; Promega) or anti-mouse IgG (1:1000; Promega) and developed with the western blotting luminol reagent ImmunoCruz (sc-2048, Santa Cruz Biotechnology, Inc.). Western blots were quantified using the Gel-Pro analyzer.

In situ hybridization

To asses which striatal subpopulation of MSNs express *He*, we performed double *in situ* hybridization for enkephalin (ENK) or tackikinin A [(Tac1, a precursor of Substance P(SP)] and immunohistochemistry for *He* as described previously (Martín-Ibáñez et al., 2010). Frozen tissue sections were air dried, fixed in 4% paraformaldehyde in PBS for 20 min at 4°C and washed in 0.1% Diethyl pyrocarbonate (DEPC; Sigma Aldrich)-PBS for 5 min. Slides were carbethoxylated in 0.1% DEPC-PBS for 10 min at r.t. Slides were washed once in 0.1% DEPC-PBS at r.t. for 1 min and twice in 0.2% DEPC-Sodium Salt Citrate (1× SSC: 150 mM NaCl, 15 mM sodium citrate) at r.t. for 2 min. Thereafter, sections were incubated with prehybridization buffer (50% formamide, 5× SSC, 5× Denhardt's solution, 250 µg/ml yeast tRNA and 500 µg/ml salmon sperm DNA) at 56ºC for 3h in a humidified chamber, and finally hybridized overnight at 56ºC with 300 µl of the same prehybridization buffer containing the oligodeoxyribonucleotide probes previously labeled with terminal deoxynucleotidyltransferase and digoxigenin (DIG)-11-dUTP (Roche). The day after, slides were washed at 56ºC with 5× DEPC-SSC 2 min, 5× DEPC-SSC 5 min, 2x DEPC-SSC 5 min, 0.2× DEPC-SSC 5 min, 50 % Formamide in 0.2× DEPC-SSC for 20 min,

Development • Supplementary information

0.2× DEPC-SSC 5 min and 1x Tris buffered saline containing with 1 % v/v of tween-20 (TBS-T) for 5 min at room temperature . To develop the signal, slides were blocked with 3% milk in TBS-T for 1h, and were incubated with the anti DIG-AP-Antibody (1:5000, Roche) in blocking buffer for 1h at r.t. Finally, in situ was developed by incubating the sections with 3.3 mg nitroblue tetrazolium and 1.65 mg bromochloroindolyl phosphate (Invitrogen S.A.) dissolved in 10 ml alkaline buffer (10X Stock: 60.5g Tris-base + 29.2g NaCl in mQ Water, pH 9.5). The enzymatic reaction was stopped by extensive rinsing in alkaline buffer with the addition of 1 mM EDTA. Next day, slides were washed with 1x Tris-EDTA buffer (TE, 10X Stock: 12.1g Tris-Base + 3.72g EDTA) and they were processed for immunohistochemistry as described previously.

Immunolabeling

Immunostainings were performed using the following antibodies: anti-*He* [1:5000 for cells and 1:1000 for tissue; polyclonal; a generous gift of Dr. Stephen T. Smale (Howard Hughes Medical Institute, Molecular Biology Institute, and Department of Microbiology and Immunology, UCLA School of Medicine, Los Angeles, CA, USA), (Hahm et al., 1998)], anti-*He* (1:50; polyclonal; Santa Cruz Biotechnology Inc.) anti-nestin (Rat 401; 1:50; polyclonal; Developmental Studies Hybridoma Bank; The University of Iowa, Iowa), anti-GFAP (1:200; monoclonal; Sigma Chemical Co.), anti-β-III-tubulin (Tuj1; 1:200; Sigma Chemical Co.), anti-MAP2 (1:500; monoclonal; Sigma Chemical Co.), anti-MAP2 (1:500; polyclonal; Abcam, Cambridge, UK), anti-NeuN (1:100; monoclonal; Merck KGaA, Darmstadt, Germany), anti- dopamine- and cAMP-regulated phosphoprotein of 32 kDa (DARPP-32; 1:500; polyclonal; BD Biosciences), anti-enkephalin (1:2000; polyclonal; ImmunoStar, Inc., Hudson, WI, USA), anti-calbindin (1:1000; monoclonal; Sigma Chemical Co.), anti-parvalbumin

Development • Supplementary information

(1:1000; polyclonal; SWANT, Bellinzona, Switzerland), anti-Choline Acetyl Transferase (ChAT; 1:500; polyclonal; Life Technologies S.A.), anti-Cleaved Caspase-3 (1:200; polyclonal; Cell Signaling Technology), anti-*Ctip2* (1:400; polyclonal: Abcam), anti-Ki67 (NCL-L-ki67-MM1; 1:100; monoclonal; Leica Microsistemas S.L.U. Barcelona), anti-Ki67 (1:50; monoclonal [SP6]; Abcam); anti-Phospho-Histone H3 (PH3; 1:200; Monoclonal; Cell Signaling Technology), anti-BrdU (1:50; monoclonal; Dako A/S, Glostrup, Denmark), GFP-FITC (1:200; polyclonal; Abcam), TUNEL (DeadEnd™ Fluorometric TUNEL System; Promega Biotech Ibérica SL, Alcobendas, Madrid) and EdU (C10420, Click-iT® EdU Alexa Fluor® 488 Flow Cytometry Assay Kit; Life Technologies S.A.).

All these antibodies were previously used and validated in (Bosch et al., 2004; Canals et al., 2004; Martín-Ibáñez et al., 2010; Pineda et al., 2005).

For histological preparations embryonic or postnatal brains were removed at specific developmental stages and were frozen in dry-ice cooled methyl-butane (Sigma Chemical Co.). Serial coronal cryostat sections (14 μm) were cut on a cryostat and collected on silane-coated slides and frozen at -20^{o}C.

Fluorescent immunolabeling was performed according to the protocol described in (Bosch et al., 2004). Briefly, cultures were fixed with 4% PFA for 20 min. Cultures and/or tissue sections were blocked for 1 h in PBS containing 0.3% Triton X-100 and 1% bovine serum albumin (BSA) to avoid non specific binding. For BrdU labeling an initial permeabilization treatment was performed before the blocking step. This was achieved by incubating cultures or tissue sections for 30 minutes or 90 minutes, respectively, in 2N HCl followed by a 20 minute wash in sodium borate 0.1M. Following the blocking step samples were incubated overnight at 4°C in PBS containing 0.3% Triton X-100 and 1% BSA with the corresponding primary antibodies. After three

Development • Supplementary information

PBS washes, cultures or tissue sections were incubated for 2 h at room temperature (r.t.) with the following secondary antibodies: Cy3-conjugated donkey anti-rabbit IgG (1:500) or Cy2-conjugated donkey anti-mouse (1:200; all from Jackson Immunoresearch Laboratories Inc., West Grove, PE, USA). Cultures or tissue sections were counterstained with 4,6'-diamidino-2-phenylindole (DAPI; Sigma Chemical Co.) and mounted in Mowiol (Calbiochem, La Jolla, CA, USA). No signal was detected in control preparations from which the primary antibody was omitted. Fluorescent photomicrographs were taken on a Leica TCS SL laser scanning confocal spectral microscope (Leica Microsistemas S.L.U.). All images were acquired as tiff files and adjustments of brightness and contrast were performed with Adobe Photoshop 6.0 (Adobe Systems Incorporated).

To analyze the cellular populations of the adult striatum, 5-6 weeks old wt and *He*$^{-/-}$ mice were transcardially perfused with 4% PFA. Brains were removed, postfixed for 2 hours at 4°C in the same solution, cryoprotected in PBS containing 30% sucrose, and frozen in dry ice-cooled methyl-butane (Sigma Chemical Co.). Serial coronal cryostat sections (30 µm thick) through the whole striatum were collected as free-floating sections in PBS and processed for diaminobenzidine immunohistochemistry as described previously (Canals et al., 2004). Briefly, endogenous peroxidases were blocked for 30–45 min in PBS containing 3% H_2O_2. Subsequently, nonspecific protein interactions were blocked with normal serum or bovine serum albumin. Samples were incubated overnight at 4ºC with the corresponding primary antibodies. Sections were washed three times in PBS and incubated with a biotinylated secondary antibody (1:200; Thermo Fisher Scientific Inc., Rockford, IL, USA) at r.t. for 2 h. The immunohistochemical reaction was developed using the ABC kit (Thermo Fisher Scientific Inc.) and visualized with diaminobenzidine. No signal was detected in control

Development • Supplementary information

preparations from which the primary antibody was omitted. Cresyl violet staining was performed as described previously (Giralt et al., 2010).

Measurement of volumes and *in vivo* cell counts

The volumes of certain brain regions were measured using ImageJ v1.33 on a computer attached to an Olympus microscope (Olympus Danmark A/S, Ballerup, Denmark). Consecutive 30 µm-thick sections (14–16 sections/animal) for adult mice and 14-µm-thick sections for embryos were viewed, and the borders of the anatomical landmarks were outlined. The volumes were calculated by multiplying the sum of all section areas (mm^2) by the distance between successive sections (0.3 mm) as described previously (Canals et al., 2004). All cell counts (EdU and Ki67 for GZ proliferation; BrdU for birth dating experiments; Cleaved Caspase 3 for cell death; Ctip2, Calbindin, DARPP-32, ChAT and Parvalbumin for striatal cell population) were genotype-blind (n: 4–6 per each condition). Nuclear stained cells were counted for BrdU, Ki67, EdU, Ctip2 and Cleaved Caspase 3. For the rest of the markers those cells showing a clear positive cytoplasm surrounding a less well-stained nucleus were counted. Unbiased stereological counts were performed using the Computer Assisted Stereology Toolbox (CAST) software (Olympus Danmark A/S). Stereological cell counts cover all striatal area for each animal. Dorso-medial (DM), dorso-lateral (DL), ventro-medial (VM) and ventro-lateral (VL) striatal areas were specifically counted along the rostrocaudal axis for DARPP-32, ENK and SP positive cells. These cell counts were also done by unbiased stereological counts using the CAST software.

The number of positive cells in the striatum, GZ or MZ was estimated using the optical dissector method (Gundersen et al., 1988). A grid size was chosen so that 10% of total striatal, GZ or MZ area was counted. The unbiased counting frame was positioned randomly on the outline of the striatum, GZ, or MZ by the software, thereby

Development • Supplementary information

creating a systematic random sample of the area. Sections were viewed under a 100x objective, and the counting field corresponded to 1,529.00 μm^2. Gundersen coefficients of error were all less than 0.10. For striatal cell counts, sections spaced 240 μm apart were analyzed. For GZ and MZ cell counts, sections spaced 140 μm apart were analyzed.

The distribution of mitosis in *He*$^{-/-}$ and wt striatum at E16.5 was analyzed as described in (Pilz et al., 2013). Briefly, E16.5 slides were stained for PH3 as described previously, and mitotic cells of the striatal GZ were classified into three types of progenitors: PH3+ cells in the border of the ventricle generated Apical progenitors (AP); PH3+ cells inside the VZ conformed Subapical progenitors (SAP) and Basal progenitors (BP) were PH3+ cells in the SVZ. PH3+ cells were counted using CAST software.

Quantification of double positive cells for *He* and D2R, D1R, ENK or SP were done by counting the number of double positive cells on five coronal sections per animal spaced 100 μm apart (*n*=3 animals per condition). Results are expressed as the percentage of *He* + cells that express D2R, D1R, ENK or SP, considering the total *He* + cells as the 100%.

Quantification of Cleaved caspase 3 + cells that were double positive for Nestin, GFAP or NeuN were done by counting the number of double positive cells on five coronal sections per animal spaced 100 μm apart (*n*=3 animals per condition). Total number of Cleaved caspase 3+ cells were considered 100%.

Automated quantification of branches, and neurite length was performed using Cell Profiler v2.8 software (pipeline available upon request), briefly, cell somas were manually selected and a secondary object recognition of morphology was performed using somas as seeds, the modules Morph/skeletonize and MeasureNeurons were then

Development • Supplementary information

used to obtain each neuron branching graph with measurements of every neurite. (GFP n=47, He=22). All the analysis was performed in a blinded fashion.

Q-PCR

Gene expression was evaluated by Q-PCR assays as previously described by Martin-Ibanez et al. (Martín-Ibáñez et al., 2010). The following TaqMan® and IDT Gene expression Assays (Applied Biosystems, Foster City, CA and Integrated DNA Technologies, BVBA, Belgium, respectively) were used: 18s, Hs99999901_s1; *Gsx2*, Mm00446650_m1; *Ascl1*, Mm03058063_m1; *Dlx1*, Mm00438424_m1; *Dlx2*, Mm00438427_m1; *Dlx5*, Mm00438430_m1; *Dlx6*, Mm01166201_m1; *Ebf1*, Mm00395519_m1; *Eos*, Mm00617657_m1; *Peg*, Mm00731061_s1; *He*, Mm00496108_m1.; *Ccne*, Mm.PT.58.8618916. To provide negative controls and exclude contamination by genomic DNA, the reverse transcriptase was omitted in the cDNA synthesis step, and the samples were subjected to the PCR reaction with each TaqMan® gene expression assay.

Analysis and quantification was performed with the Comparative Quantitation Analysis program of the MxPro™ Q-PCR analysis software version 3.0 (Stratagene, La Jolla, CA, USA), using the 18S gene expression as internal loading control. All Q-PCR assays were performed in duplicate and repeated for at least three independent experiments. The results were expressed as relative levels with respect to the expression of the same gene in E14.5 for developmental studies or the control vector over-expressing cells considered as 100%.

Primary striatal culture and transfection

E14.5 fetal brains from wt embryos were excised and the LGEs were dissected and cultured as previously described (Martín-Ibáñez et al., 2010). For *He* over-expression

Development • Supplementary information

studies, cells were transfected with the MSCV-*He*-IRES-eGFP plasmid, or with the MSCV-IRES-eGFP plasmid as a control (Zhang et al., 2007). Primary cultures were transfected 24 hours after seeding with 0.5 µg of the corresponding plasmids per well (24-well plate). The transfection was performed using Lipofectamine LTX (Life Technologies S.A.), accordingly to the manufacturer instructions, which results in a transfection efficiency of 0.5-1% of the cells. Three days after transfection cells were fixed with 4% PFA for immunocytochemistry analysis. We counted the number of *He* or eGFP overexpressing cells per coverslip that co-localized with different markers, such as calbindin, DARPP-32 and enkephalin. The results were expressed as the percentage of transfected cells co-localizing with the different markers with respect to the total number of transfected cells. These experiments were performed with at least 3-4 independent LGE primary cultures.

Cell transplants

Prior to transplantation, eGFP mice derived neurospheres were transduced with either *He* or eGFP were harvested and resuspended in PBS. P2-P3 neonatal mice were anesthetized by hypothermia, placing them on ice until cessation of movement. Unilateral striatal injections were performed using a stereotaxic apparatus (Davis Kopf Instruments, Tujunga, CA, USA) and a 10 µl Hamilton syringe with a 33 gauge needle (Hamilton, Reno, NV), setting the following coordinates (millimeters): AP, +2.3, L, +1.4 from lambda and DV, -1.8 from dura. Every animal received 10000 cells diluted in 1 µl of PBS. Upon completion of stereotaxic surgery, pups were warmed, monitored for 1h to ensure recovery and then returned to the housing facility for 2 or 4 weeks.

Quantification of transplanted cells was performed by counting the number of GFP^{+}/DARPP-32 + neurons on five coronal sections per animal spaced 100 µm apart

Development • Supplementary information

(*n*=3 animals per condition). All GFP positive cells were examined for DARPP-32 + immunostaining.

Mouse Behavior

Swimming task

The apparatus consisted of a transparent perspex extended swimming tank (100 cm long, 10 cm wide with walls measuring 40 cm high). Water level was 20 cm from floor to surface, and it was maintained at 26°C ± 1. A black screen surrounded the tank to avoid the vision of distal cues. Testing conditions were carried out in dimly light conditions (100 lux). The mice were placed in an extreme of the swimming tank facing away from a visible escape platform (10 cm wide, 10 cm long and with a 10 cm high with the top surface 0.5 cm above the water level) at one end of the tank. The time required to reach the platform (escape latencies) in these trials was recorded. Two blocks of three trials with an inter-block interval of 24 h were performed.

Balance beam

A beam consisted of a long steel cylinder (50 cm) with a 50 mm-square cross-section and a 15 mm-round diameter. The beam was placed horizontally, 50 cm above the bench surface, with each end mounted on a narrow support. Animals were allowed to walk along the beam until they reach 30 cross-sections (5 cm each), while their latency to fall and number of falls were measured.

Rotarod

Acquisition of a motor coordination task was further evaluated on the rotarod apparatus at fixed rotations per minute (rpm). In brief, animals at 5 weeks of age were trained at constant speed (24 rpm) for 60 sec. We performed three trials per day for two

Development • Supplementary information

consecutive days; and the latency to fall and the number of falls during 60 sec was recorded.

Footprint test

Mice were trained to walk in a corridor that was 50 cm long and 7 cm wide. The forefeet and hindfeet of the mice were painted with non-toxic red and blue ink, respectively, and then given one run. The footprint pattern was analyzed for the general pattern and stride length was measured as the average distance of forward movement between each stride, and the forebase and hindbase widths were measured as the perpendicular distance between the left and right footprints of a given step.

Development • Supplementary information

References

Bertran-Gonzalez, J., Bosch, C., Maroteaux, M., Matamales, M., Hervé, D., Valjent, E. and Girault, J.-A. (2008). Opposing patterns of signaling activation in dopamine D1 and D2 receptor-expressing striatal neurons in response to cocaine and haloperidol. *J. Neurosci.* **28**, 5671–85.

Bosch, M., Pineda, J. R., Suñol, C., Petriz, J., Cattaneo, E., Alberch, J. and Canals, J. M. (2004). Induction of GABAergic phenotype in a neural stem cell line for transplantation in an excitotoxic model of Huntington's disease. *Exp. Neurol.* **190**, 42–58.

Cai, Q., Dierich, A., Oulad-Abdelghani, M., Chan, S. and Kastner, P. (2009). Helios deficiency has minimal impact on T cell development and function. *J. Immunol.* **183**, 2303–11.

Canals, J. M., Pineda, J. R., Torres-Peraza, J. F., Bosch, M., Martín-Ibañez, R., Muñoz, M. T., Mengod, G., Ernfors, P. and Alberch, J. (2004). Brain-derived neurotrophic factor regulates the onset and severity of motor dysfunction associated with enkephalinergic neuronal degeneration in Huntington's disease. *J. Neurosci.* **24**, 7727–39.

Giralt, A., Friedman, H. C., Caneda-Ferrón, B., Urbán, N., Moreno, E., Rubio, N., Blanco, J., Peterson, A., Canals, J. M. and Alberch, J. (2010). BDNF regulation under GFAP promoter provides engineered astrocytes as a new approach for long-term protection in Huntington's disease. *Gene Ther.* **17**, 1294–308.

Gong, S., Zheng, C., Doughty, M. L., Losos, K., Didkovsky, N., Schambra, U. B., Nowak, N. J., Joyner, A., Leblanc, G., Hatten, M. E., et al. (2003). A gene expression atlas of the central nervous system based on bacterial artificial chromosomes. *Nature* **425**, 917–925.

Gundersen, H. J., Bagger, P., Bendtsen, T. F., Evans, S. M., Korbo, L., Marcussen, N., Møller, A., Nielsen, K., Nyengaard, J. R. and Pakkenberg, B. (1988). The new stereological tools: disector, fractionator, nucleator and point sampled intercepts and their use in pathological research and diagnosis. *APMIS* **96**, 857–81.

Hahm, K., Cobb, B. S., McCarty, A. S., Brown, K. E., Klug, C. A., Lee, R., Akashi, K., Weissman, I. L., Fisher, A. G. and Smale, S. T. (1998). Helios, a T cell-restricted Ikaros family member that quantitatively associates with Ikaros at centromeric heterochromatin. *Genes Dev.* **12**, 782–96.

Kim, H.-J., Barnitz, R. A., Kreslavsky, T., Brown, F. D., Moffett, H., Lemieux, M. E., Kaygusuz, Y., Meissner, T., Holderried, T. A. W., Chan, S., et al. (2015). Stable inhibitory activity of regulatory T cells requires the transcription factor Helios. *Science (80-.).* **350**, 334–339.

Lange, C., Huttner, W. B. and Calegari, F. (2009). Cdk4/cyclinD1 overexpression in neural stem cells shortens G1, delays neurogenesis, and promotes the generation and expansion of basal progenitors. *Cell Stem*

Cell **5**, 320–31.

Martín-Ibáñez, R., Crespo, E., Urbán, N., Sergent-Tanguy, S., Herranz, C., Jaumot, M., Valiente, M., Long, J. E., Pineda, J. R., Andreu, C., et al. (2010). Ikaros-1 couples cell cycle arrest of late striatal precursors with neurogenesis of enkephalinergic neurons. *J. Comp. Neurol.* **518**, 329–51.

Naldini, L., Blömer, U., Gage, F. H., Trono, D. and Verma, I. M. (1996). Efficient transfer, integration, and sustained long-term expression of the transgene in adult rat brains injected with a lentiviral vector. *Proc. Natl. Acad. Sci. U. S. A.* **93**, 11382–8.

Okabe, M., Ikawa, M., Kominami, K., Nakanishi, T. and Nishimune, Y. (1997). “Green mice” as a source of ubiquitous green cells. *FEBS Lett.* **407**, 313–9.

Pilz, G.-A., Shitamukai, A., Reillo, I., Pacary, E., Schwausch, J., Stahl, R., Ninkovic, J., Snippert, H. J., Clevers, H., Godinho, L., et al. (2013). Amplification of progenitors in the mammalian telencephalon includes a new radial glial cell type. *Nat. Commun.* **4**, 2125.

Pineda, J. R., Canals, J. M., Bosch, M., Adell, A., Mengod, G., Artigas, F., Ernfors, P. and Alberch, J. (2005). Brain-derived neurotrophic factor modulates dopaminergic deficits in a transgenic mouse model of Huntington’s disease. *J. Neurochem.* **93**, 1057–68.

Takahashi, T., Nowakowski, R. S. and Caviness, V. S. (1992). BUdR as an S-phase marker for quantitative studies of cytokinetic behaviour in the murine cerebral ventricular zone. *J. Neurocytol.* **21**, 185–97.

Takahashi, T., Nowakowski, R. S. and Caviness, V. S. (1995). The cell cycle of the pseudostratified ventricular epithelium of the embryonic murine cerebral wall. *J. Neurosci.* **15**, 6046–57.

Urbán, N., Martín-Ibáñez, R., Herranz, C., Esgleas, M., Crespo, E., Pardo, M., Crespo-Enríquez, I., Méndez-Gómez, H. R., Waclaw, R., Chatzi, C., et al. (2010). Nolz1 promotes striatal neurogenesis through the regulation of retinoic acid signaling. *Neural Dev.* **5**, 21.

Zhang, Z., Swindle, C. S., Bates, J. T., Ko, R., Cotta, C. V and Klug, C. A. (2007). Expression of a non-DNA-binding isoform of Helios induces T-cell lymphoma in mice. *Blood* **109**, 2190–7.

Development • Supplementary information

SUPPLEMENTARY FIGURES

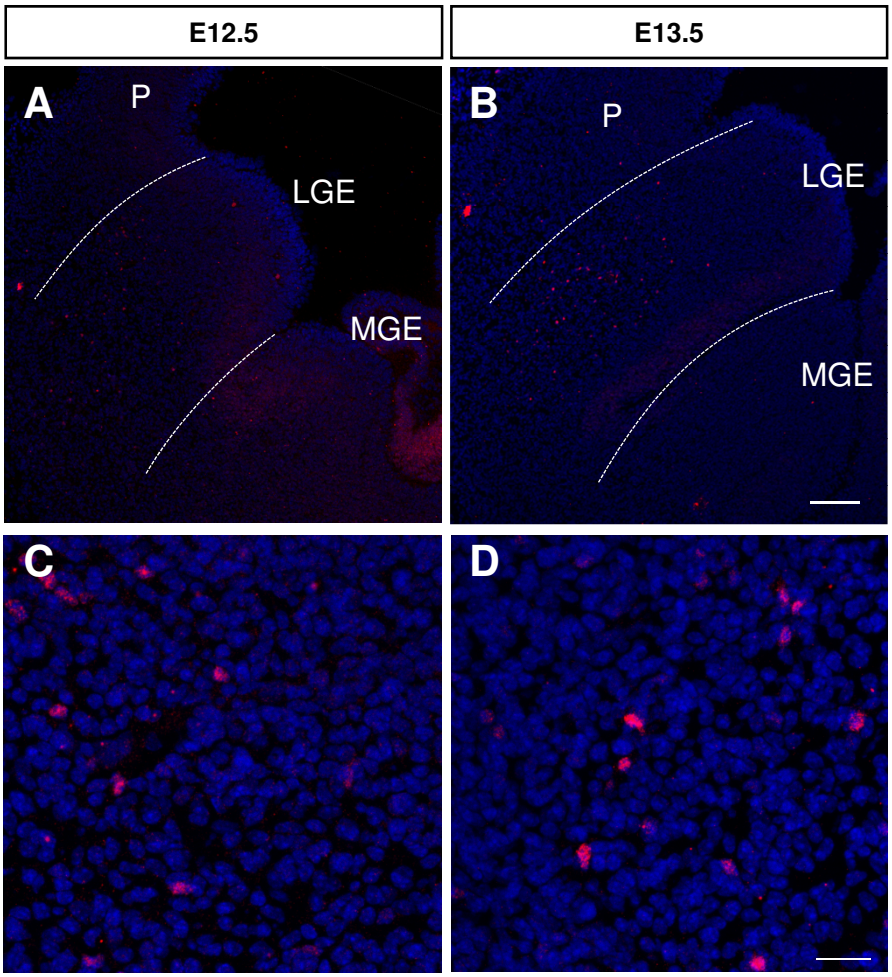

Figure S1. *He* is expressed at early embryonic developmental stages in scattered cells. (**A,C**) Immunohistochemistry for *He* at E12.5 at low (**A**) or high magnification (**C**). (**B,D**) Immunohistochemistry for *He* at E13.5 at low (**B**) or high magnification (**D**). Scale bars; A-B; 100 μm, C-D; 20 μm.

Development • Supplementary information

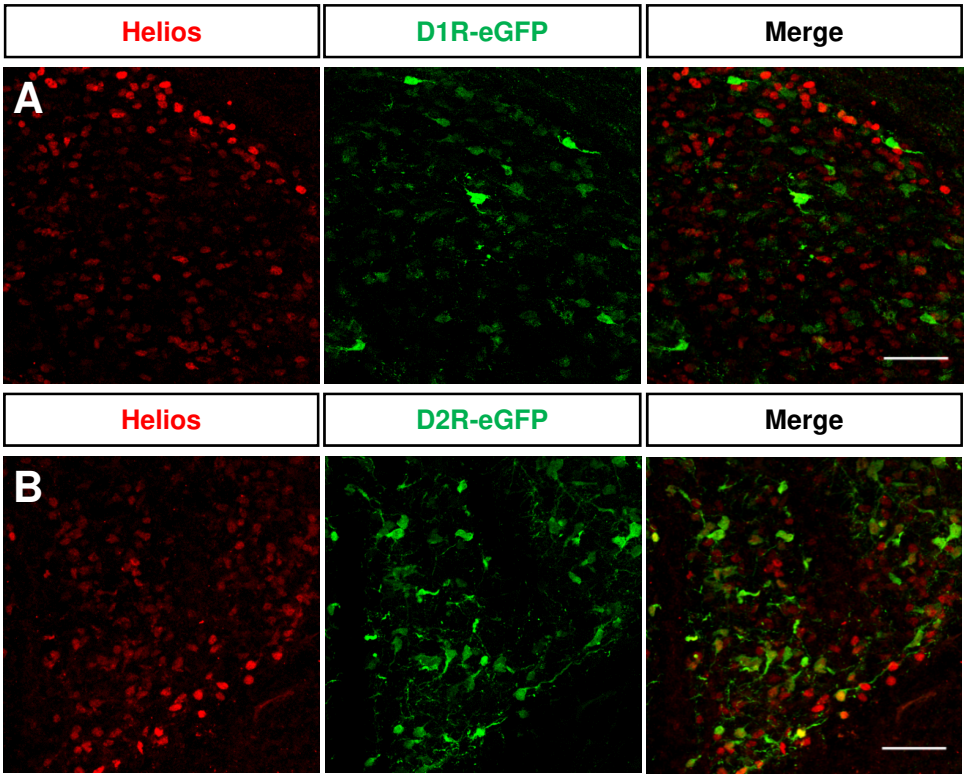

Figure S2. *He* mainly co-localizes with D2R + neurons in the striatum. (**A**) Double immunohistochemistry against *He* and GFP in the D1R-eGFP mice showing few double stained cells. This representative image is taken from de dorsolateral striatum at P3. (**B**) Double immunohistochemistry against *He* and GFP in the D2R-eGFP mice showing a higher percentage of *He* expressing cells co-localizing with D2R positive neurons. This representative image is taken from de ventrolateral striatum at P3. Scale bars: 50μm.

Development • Supplementary information

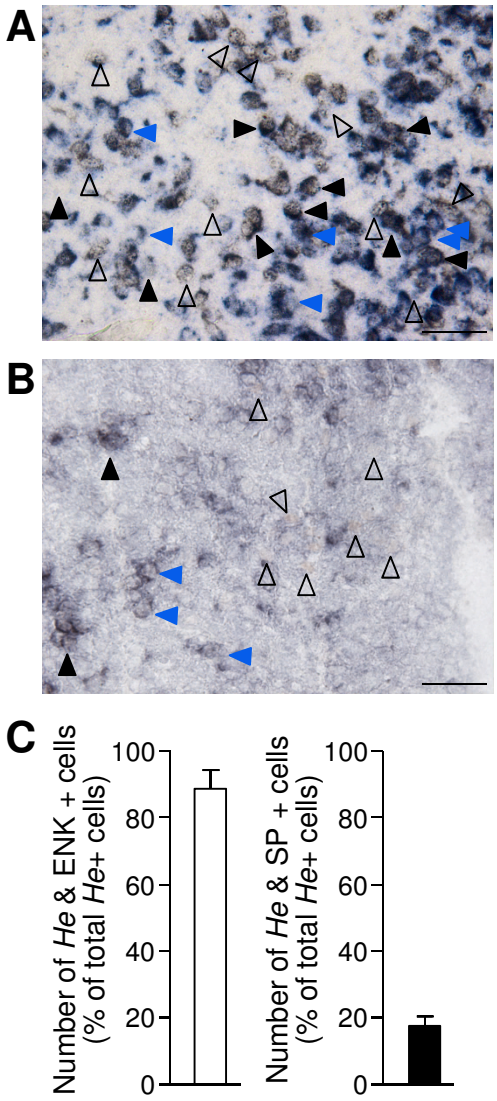

Figure S3. Helios is mainly expressed by ENK + neurons in the striatum. (**A**) Double *in situ* for ENK (dark blue) and *He* immunohistochemistry (brown) show a high percentage of colocalization (black closed arrowheads) but few *He* + cells were not ENKergic neurons (open arrowheads). In addition, some ENK + neurons were negative for *He* (blue closed arrowheads). This representative image is taken from the dorsomedial striatum at P7. (**B**) Double *in situ* for tachykinin A, the precursor of substance P, (dark blue) and *He* immunohistochemistry (brown) show low percentage of colocalization (black closed arrowheads) but many single labeled *He* + cells (open arrowheads). In addition, many tachykinin A + neurons were negative for *He* (blue closed arrowheads). This representative image is taken from the dorsolateral striatum at P7. Scale bars; 50 μm. (**C**) Quantification of the percentage of *He*+ cells that co-express ENK or SP.

Development • Supplementary information

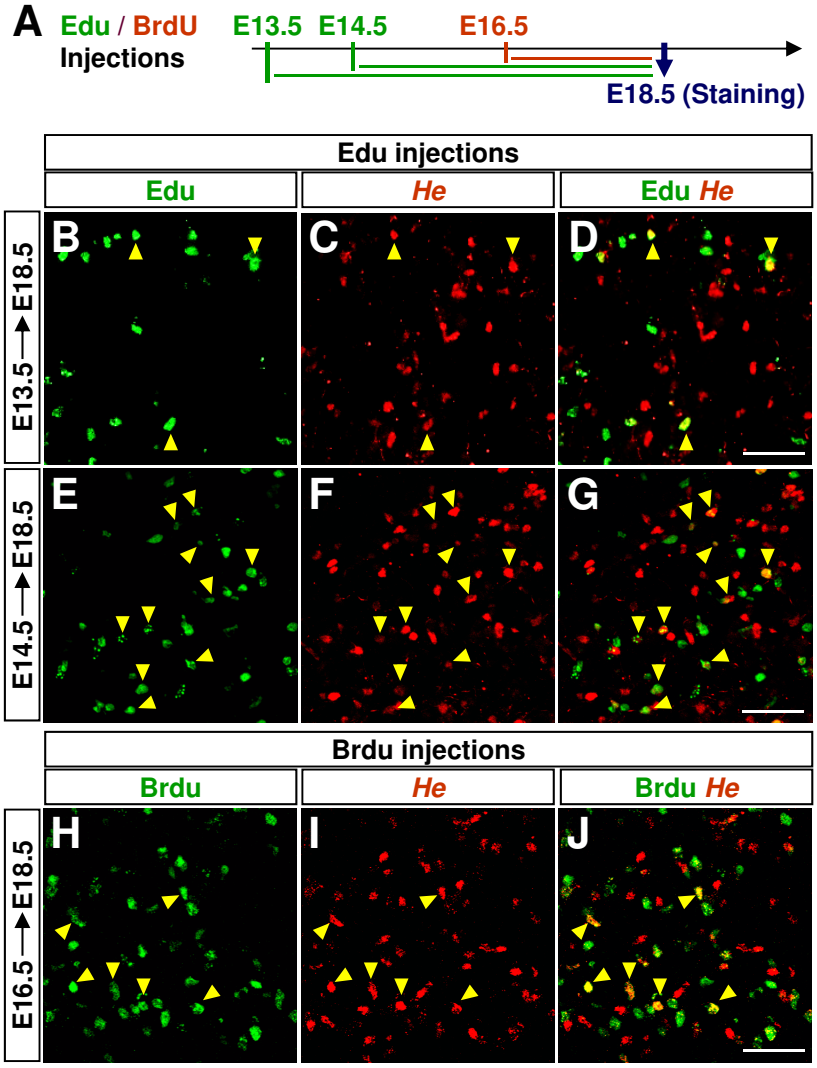

Figure S4. *He* is expressed by cells generated at late striatal neurogenic stages. (**A**) Schematic representation of double EdU and BrdU injections performed at E13.5, E14.5 and E16.5, respectively. To analyze the birth-date of *He* expressing cells, double immunohistochemistry against EdU or BrdU and *He* was performed at E18.5. (**B-D**) Double immunohistochemistry against EdU and *He* demonstrated that few of the *He*-positive cells are generated at E13.5. Yellow arrowheads point to double positive cells in a representative image taken in the mid-striatum. Scale bar: 50 μm. (**E-G**) Double immunohistochemistry against EdU and *He* demonstrated that a higher percentage of *He*-positive cells are generated at E14.5. Yellow arrowheads point to double positive cells in a representative image taken in the mid-striatum. Scale bar: 50 μm. (**H-J**) Double immunohistochemistry against BrdU and *He* demonstrated that some *He*-positive cells are generated at E16.5. Yellow arrowheads point to double positive cells in a representative image taken in the mid-striatum. Scale bar: 50 μm.

Development • Supplementary information

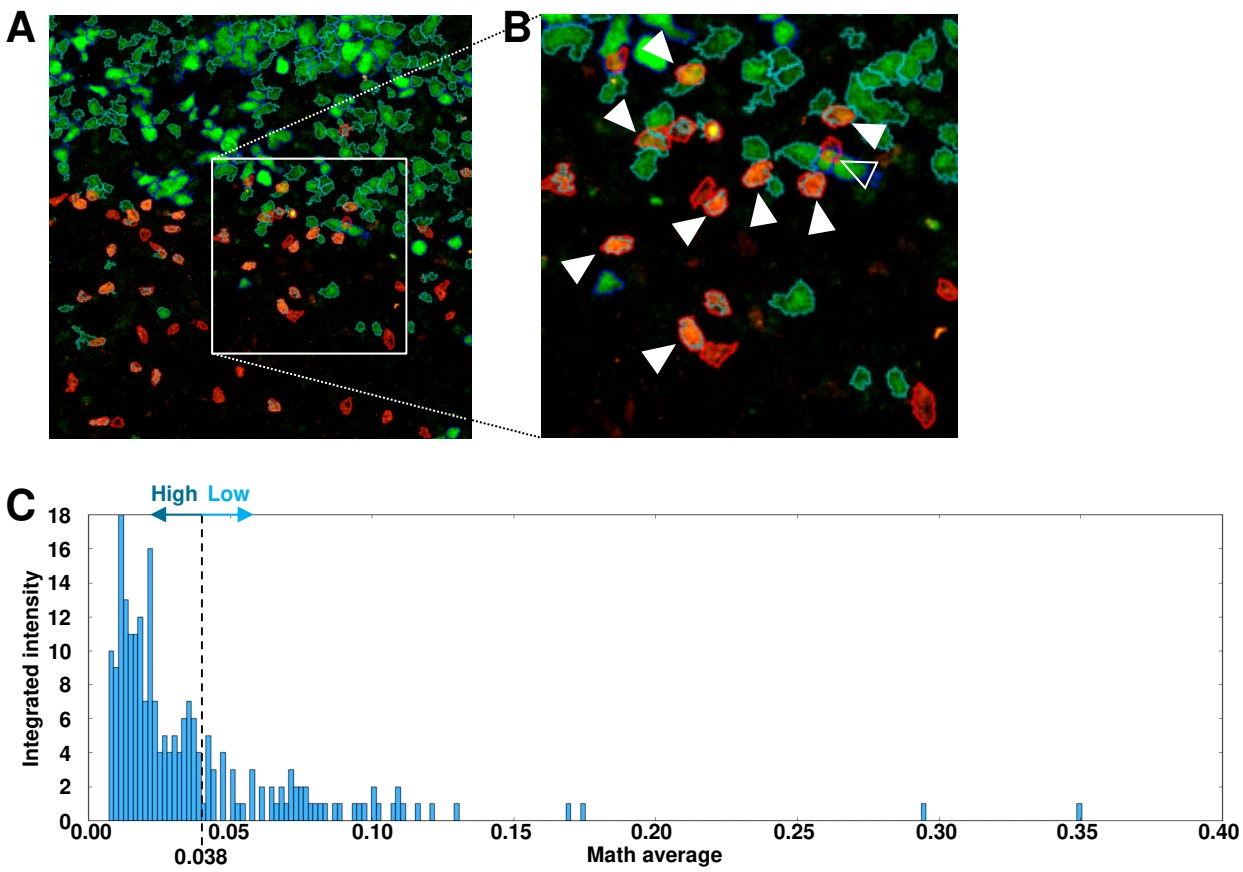

Figure S5. High and low Ki67 expressing cells were analyzed by using the Cell Profiler program. (**A**) Representative picture of the automatic detection of high expressing Ki67 cells (dark blue), low expressing Ki67 cells (light blue) and He expressing cells (red). (**B**) As evidenced in the image only 1 cell with high expression of Ki67 partially overlaps with He expression (open arrowhead), whereas the rest of Ki67/He+ve cells are low expressing (close arrowhead). (**C**) Graft representing the intensity of Ki67 expressing cells and cut off at 0.038.

Development • Supplementary information

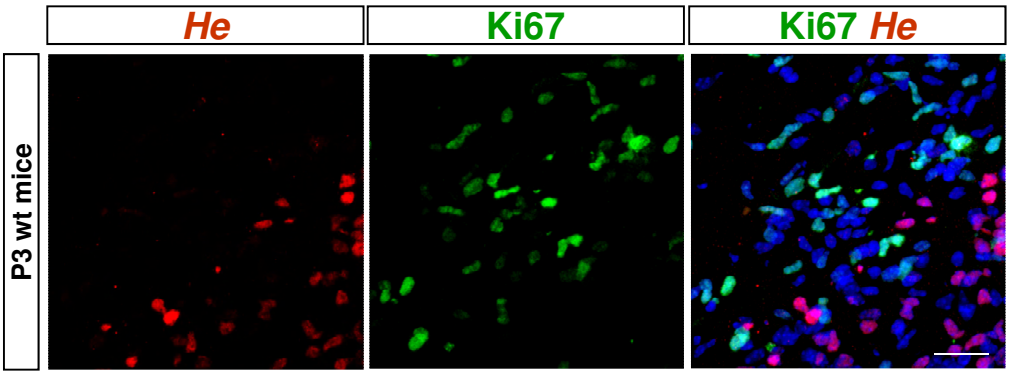

Figure S6. *He* is not expressed in proliferative cells at postnatal stages. Representative images at the GZ-MZ border of the ventro-medial striatum showing lack of co-localization between *He* and the proliferative marker Ki67 at P3. Scale bar: 20 µm.

Development • Supplementary information

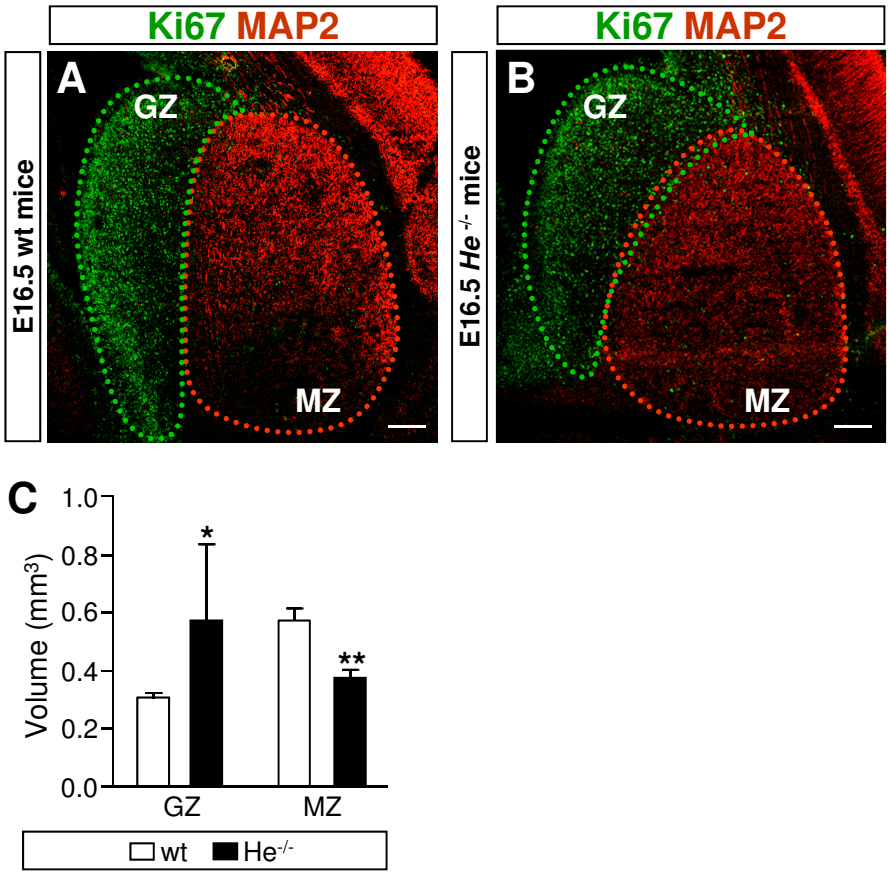

Figure S7. *He*$^{-/-}$ mice show an increase in the volume of the proliferative area. (**A-B**) Representative pictures of E16.5 striatal primordium double stained for Ki67 and MAP2 in wt and *He*$^{-/-}$ mice. Note the enlargement observed in the Ki67 positive proliferative zone of *He*$^{-/-}$ mice compared to wt mice. Proliferative and non-proliferative areas are delimited by dotted lines in green and red, respectively. Scale bar: 200 μm. (**C**) Quantification of the volume of GZ and MZ of wt and *He*$^{-/-}$ mice at E16.5. Results represent the mean ± s.e.m. of 4-6 mice per condition. Statistical analysis was performed using Student's t-test; *$p < 0.05$, **$p<0.005$.

Development • Supplementary information

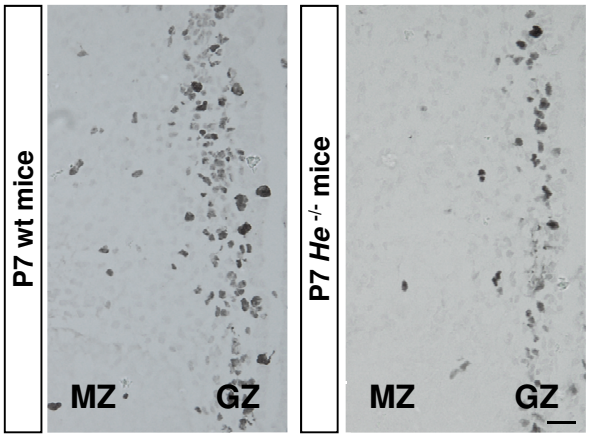

Figure S8. The number of proliferative progenitors in the GZ is reduced in the absence of *He* at P7. Representative photomicrographs of Ki67+ cells in the dorsal GZ of wt and *He*$^{-/-}$ mice at P7. Scale bar: 20 μm

Development • Supplementary information

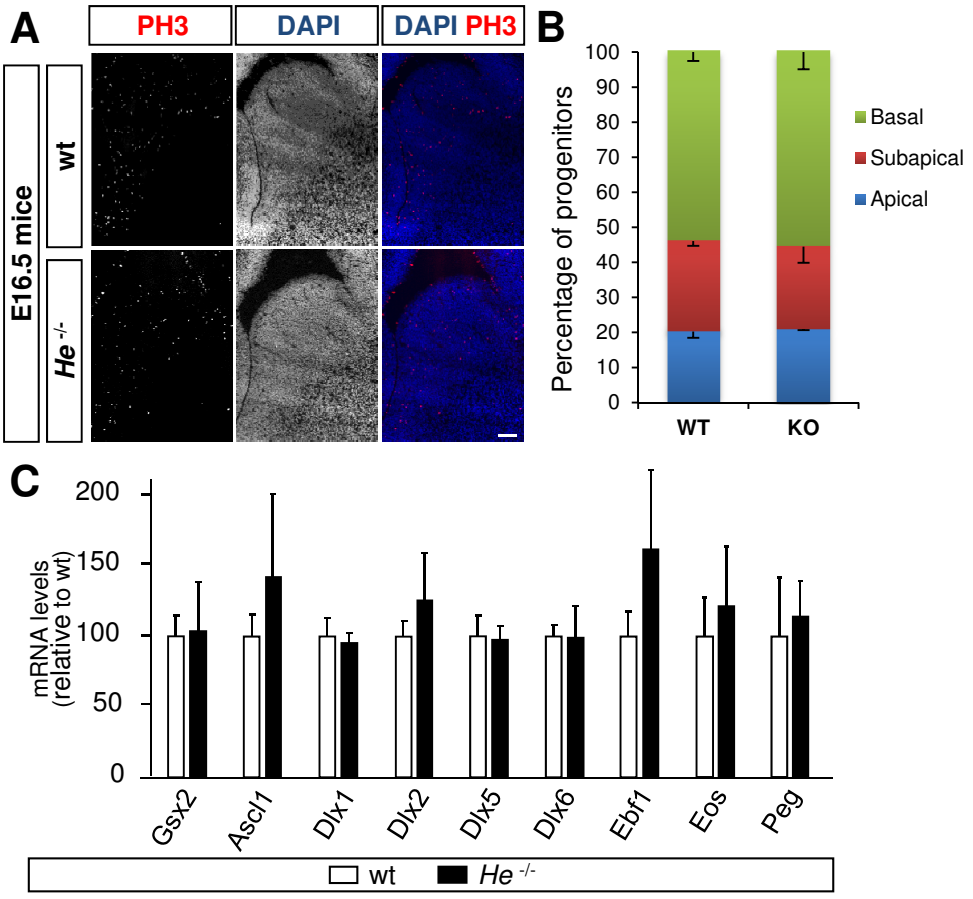

Figure S9. *He* does not affect radial glia subtypes. (**A-B**) Immunohistochemistry for PH3 in *He*$^{-/-}$ and wt striatal coronary sections at E16.5 and quantification of the percentage of basal, subapical and apical progenitors. Basal progenitors are predominant in the striatal GZ at E16.5 with no changes in the percentage between *He*$^{-/-}$ and wt conditions. Scale bar: 200 μm. Results represent the mean ± s.e.m. of 4-6 mice per condition. Statistical analysis was performed using Student's t-test; *p < 0.05, ***p<0.001. (**C**) We analyzed the levels of mRNA expression of several progenitor markers in the striatum of E16.5 wt and *He*$^{-/-}$ mice by Q-PCR. No differences are observed between genotypes. Results represent the mean ± s.e.m. of 4-5 LGEs from each genotype.

Development • Supplementary information

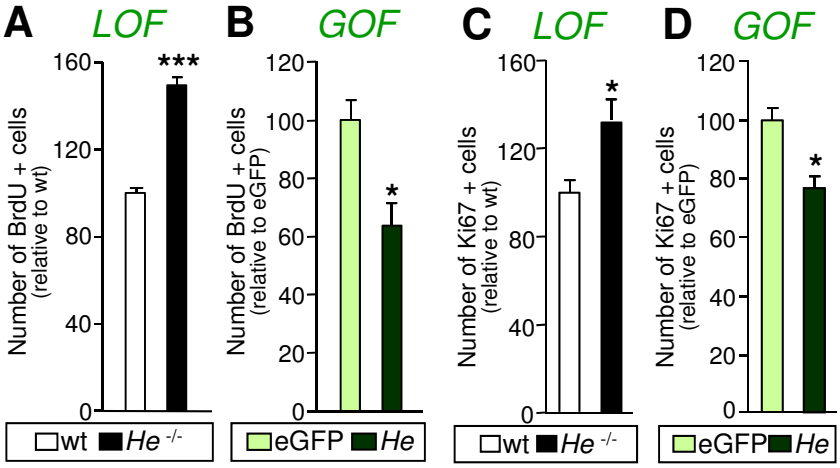

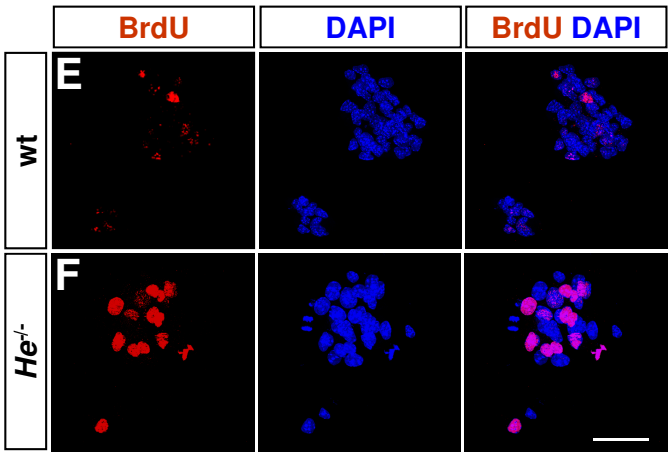

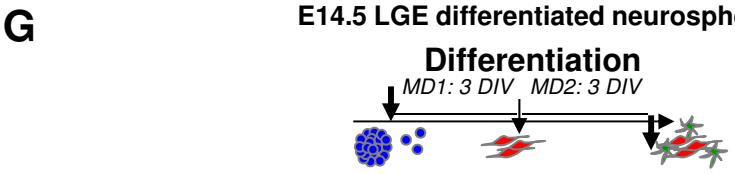

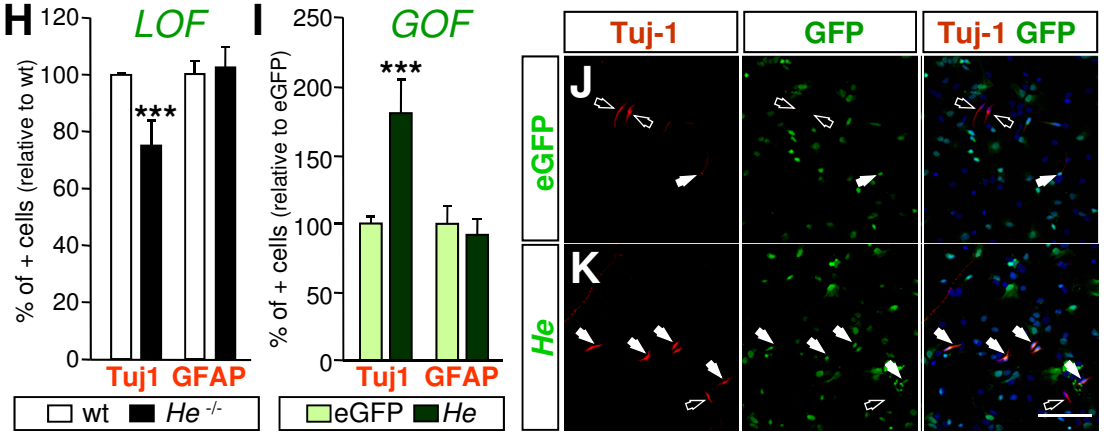

Development • Supplementary information

Figure S10. *He* regulates NPC proliferation and neurogenesis *in vitro.* (**A**) (**A**) Loss of function (*LOF*) experiments demonstrated that more NPCs incorporate BrdU in neurospheres derived from *He*$^{-/-}$ mice compared to wt mice. (**B**) Gain of function (*GOF*) experiments showed that *He* over-expression in wt neurospheres reduced the number of NPCs that incorporate BrdU compared to the control eGFP over-expression cultures. (**C**) *LOF* experiments demonstrated an increase in Ki67 positive proliferating cells in the absence of *He*. (**D**) *GOF* experiments showed that *He* over-expression reduced the number of Ki67-positive NPCs compared to neurosphere cultures over-expressing eGFP alone. (**E-F**) Representative images of BrdU incorporation in wt (**E**) and *He*$^{-/-}$ (**F**) mice derived neurospheres. Note the increase in the number of cells that are positive for BrdU in the *He*$^{-/-}$ NPCs. Scale bar: 50 μm. (**G**) Schematic timeline of the differentiation of E14.5 LGE derived neurospheres. (**H**) *LOF* experiments prove that *He* loss produced a significant reduction in the number of β-III-tubulin (Tuj-1)+ neurons without affecting the number of GFAP+ astrocytes. (**I**) *GOF* experiments show that *He* over-expression increased significantly the number of β-III-tubulin (Tuj-1)+ neurons but did not modify the number of GFAP+ astrocytes. (**J-K**) Representative photomicrographs of differentiated NSCs cultures over-expressing *He* (*He*) (**J**) or the control eGFP plasmid (**K**), double stained for eGFP and the neuronal differentiation marker β-III-tubulin (Tuj-1). White arrows point to double stained cells and open arrows point to single Tuj-1+ cells. Scale bar: 60 μm. Results represent the mean ± s.e.m. of 4-5 LGE-derived neurosphere cultures. Statistical analysis was performed using Student's t-test; *$p < 0.05$, ***$p < 0.001$.

Development • Supplementary information

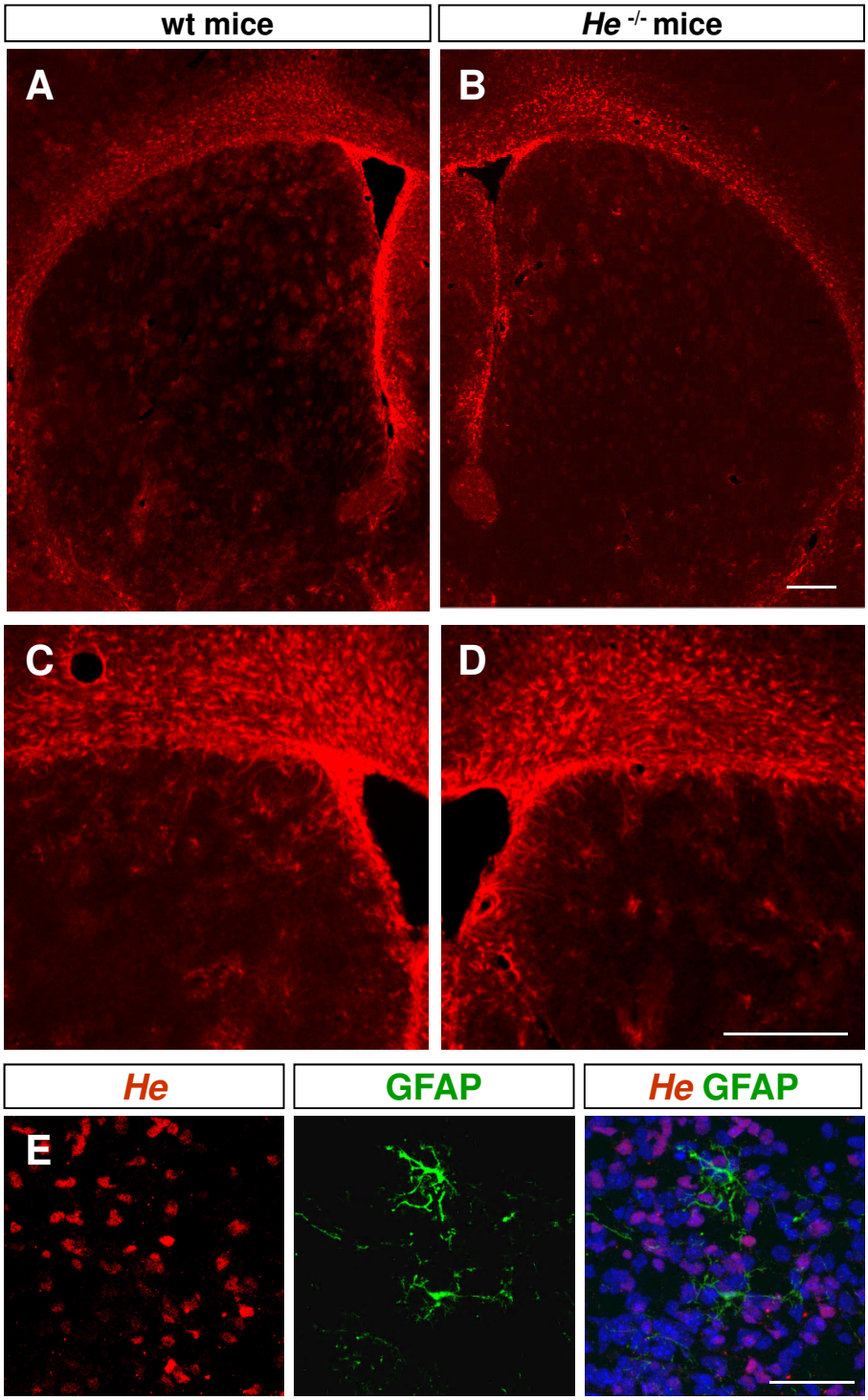

Figure S11. *He* is not involved in the generation of GFAP-positive astrocytes. (**A-D**) Striatal coronal sections immunostained for GFAP in wt (**A,C**) and *He*$^{-/-}$ adult mice (**B,D**) at low and high magnification (**A-B** and **C-D**, respectively). No differences are observed between the two genotypes. Scale bar: 200 μm. (**E)** Representative photomicrograph showing the lack of co-localization between *He* and the glial marker GFAP in a coronal dorsomedial striatal section at P3 Scale bar: 30 μm.

Development • Supplementary information

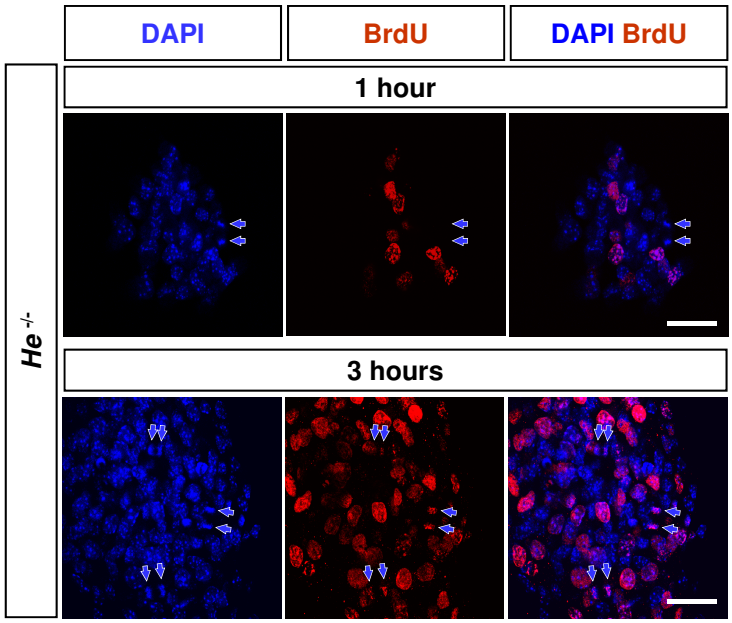

Figure S12. Analysis of the mitotic index. Representative image of BrdU and DAPI immunocytochemistry of neurospheres during the analysis of the mitotic BrdU labeling index. Note that after 1 hour almost all mitotic cells are negative for BrdU whereas after 3 hours almost all of them are positive. Double arrows indicate mitotic cells. Scale bar: 50 μm.

Development • Supplementary information

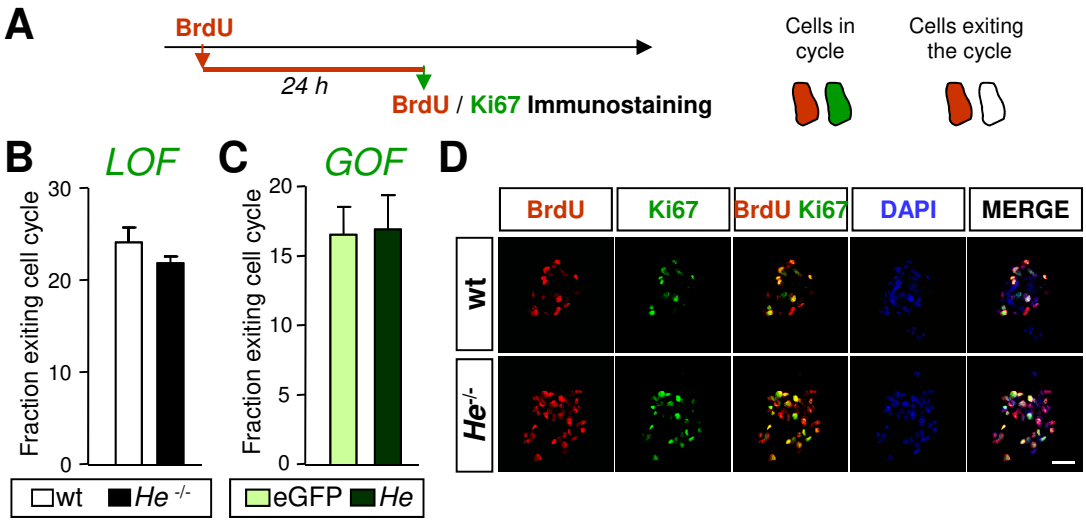

Figure S13. Helios does not affect the fraction of cells exiting the cell cycle. (**A**) Schematic timeline of cell cycle exit experiments in which double staining for BrdU and Ki67 was performed in NPCs cultures after a 24h pulse of BrdU. (**B**) *LOF* experiments showed no differences in cell cycle exit between *He*$^{-/-}$ and wt mice-derived neurospheres. (**C**) *GOF* experiments revealed that *He* over-expression does not produce changes in cell cycle exit. (**D**) Representative images showing no differences in cell cycle exit between wt and *He*$^{-/-}$ mice-derived neurospheres. Scale bar: 50 μm.

Development • Supplementary information

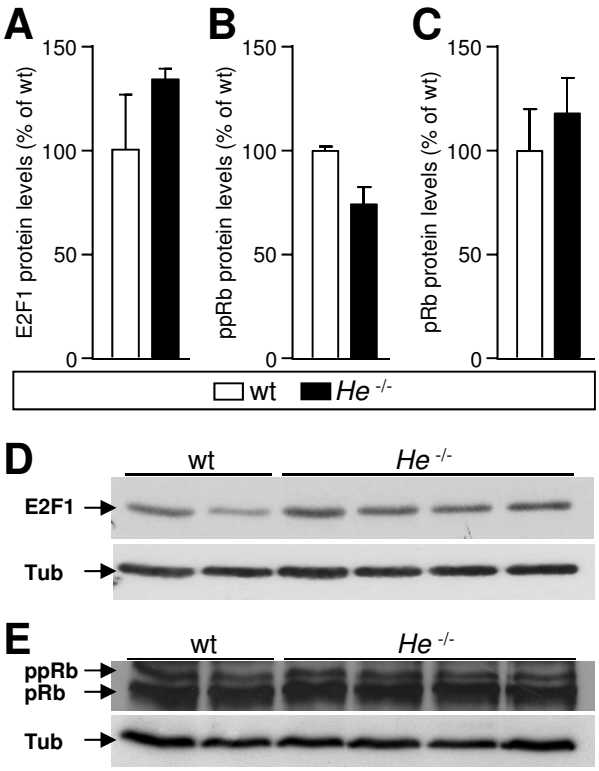

Figure S14. He does not regulate the levels of E2F1 or hyper or hypo-phosphorylated retinoblastoma (Rb). (**A**) Lack of differences in the levels of E2F1 between wt and *He*$^{-/-}$ mice. (**B-C**) Similarly, the levels of hyper-phosphorylated Retinoblastoma (ppRb; **B**) or hypo-phosphorylated Retinoblastoma (pRb; **C**) do not show differences between phenotypes. Results represent the mean ± s.e.m. of 4-5 LGE-derived neurosphere cultures. Statistical analysis was performed using Student's t-test. (**D**) Representative bands of E2F1 in wt and *He*$^{-/-}$ mice. (**E**) Representative bands of ppRb and pRb in wt and *He*$^{-/-}$ mice. Tub; tubulin.

Development • Supplementary information

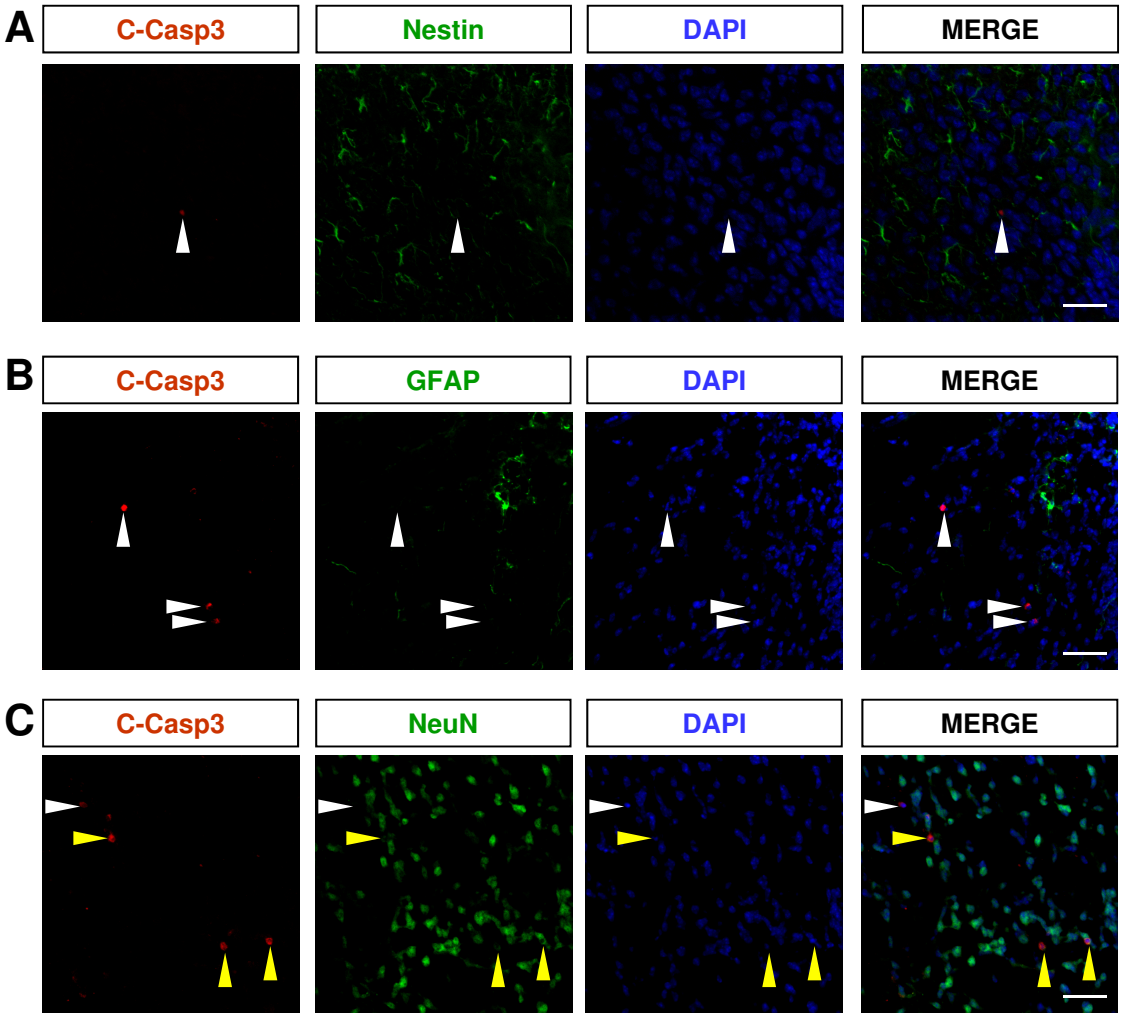

Figure S15. Cell death induced by *He* loss is detected in neurons but not in NPCs or glial cells. (**A**) Representative photomicrographs of striatal P3 coronal sections showing a lack of co-localization of Nestin and cleaved caspase 3 (C-casp3) in the dorsal striatum. White arrowheads point to C-casp3 single labeled cells. Scale bar: 30 μm. (**B**) Representative photomicrographs of striatal P3 coronal sections showing lack of co-localization of GFAP and cleaved caspase 3 (C-casp3) in the dorsal striatum. White arrowheads point to C-casp3 single labeled cells. Scale bar: 30 μm. (**C**) Representative photomicrographs of striatal P3 coronal sections showing co-localization of NeuN and cleaved caspase 3 (C-casp3) in the dorsal striatum. White arrowheads point to C-casp3 single labeled cells. Yellow arrowheads point to C-casp3 and NeuN double labeled cells. Scale bar: 30 μm.

Development • Supplementary information

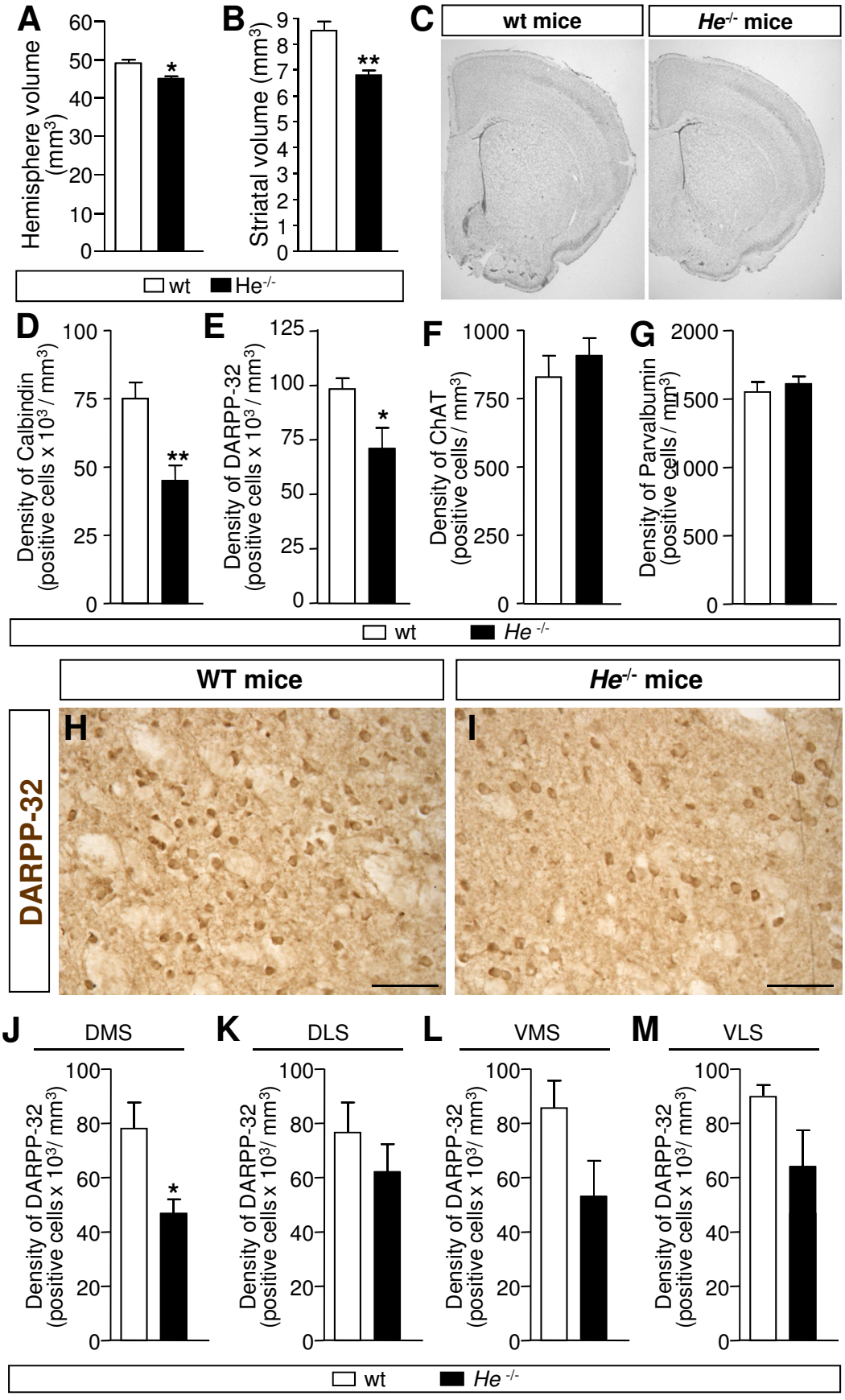

Development • Supplementary information

Figure S16. *He* loss produces a decrease of MSN density at the DMS. (**A,C**) Brain hemisphere volume was slightly reduced in *He*$^{-/-}$ mice compared to wt mice. (**B,C**) Striatal volume was significantly reduced in approximately a 20% in *He*$^{-/-}$ mice compared to wt mice. (**C**) Representative photomicrographs of cresyl violet staining of wt and *He*$^{-/-}$ mice brains showing the reduction in striatal volume. (**D**) Density of striatal calbindin+ cells is reduced in *He*$^{-/-}$ adult mice compared to wt adult mice. (**E**) Density of striatal DARPP-32+ cells is reduced in *He*$^{-/-}$ adult mice compared to wt adult mice. (**F**) The density of striatal ChAT+ cells is not altered between wt and *He*$^{-/-}$ adult mice. (**G**) The density of striatal Parvalbumin+ cells is not altered between wt and *He*$^{-/-}$ adult mice. (**H-I**) Representative photomicrographs of DARPP-32 immunohistochemistry in the dorsomedial striatum of wt (**H**) and *He*$^{-/-}$ (**I**) mice. Scale bar: 50 µm. (**J-M**) Density of striatal DARPP-32+ cells is specifically reduced in the DMS (**J**) in *He*$^{-/-}$ adult mice compared to wt adult mice. No differences are found in the DLS (**K**), VMS (**L**) and VLS (**M**) between both genotypes**.** DMS, dorsomedial striatum; DLS, dorsolateral striatum; VMS, ventromedial striatum; VLS, ventrolateral striatum.

Development • Supplementary information

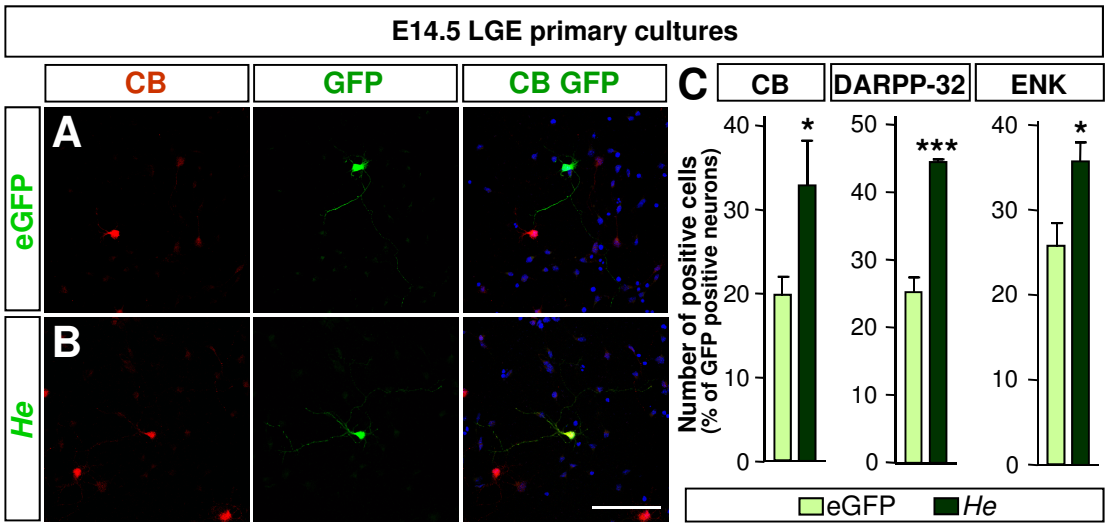

Figure S17. *He* induces a striatal MSN phenotype. (**A-B**) Representative photomicrographs showing double immunocytochemistry for eGFP and calbindin (CB) in primary striatal cultures overexpressing eGFP alone (**A**) or eGFP-*He* (*He*) (**B**). (**C**) Quantification of the number of *He* and eGFP positive cells co-localizing with CB, DARPP-32 and ENK. The bars in the graph represent the percentage of transfected cells positive for each marker out of the total number of transfected eGFP-positive cells. Scale bar: 50 μm. Results represent the mean ± s.e.m. of 4-5 LGE- primary cultures. Statistical analysis was performed using Student's *t*-test; *p < 0.05, ***p < 0.001.

Development • Supplementary information

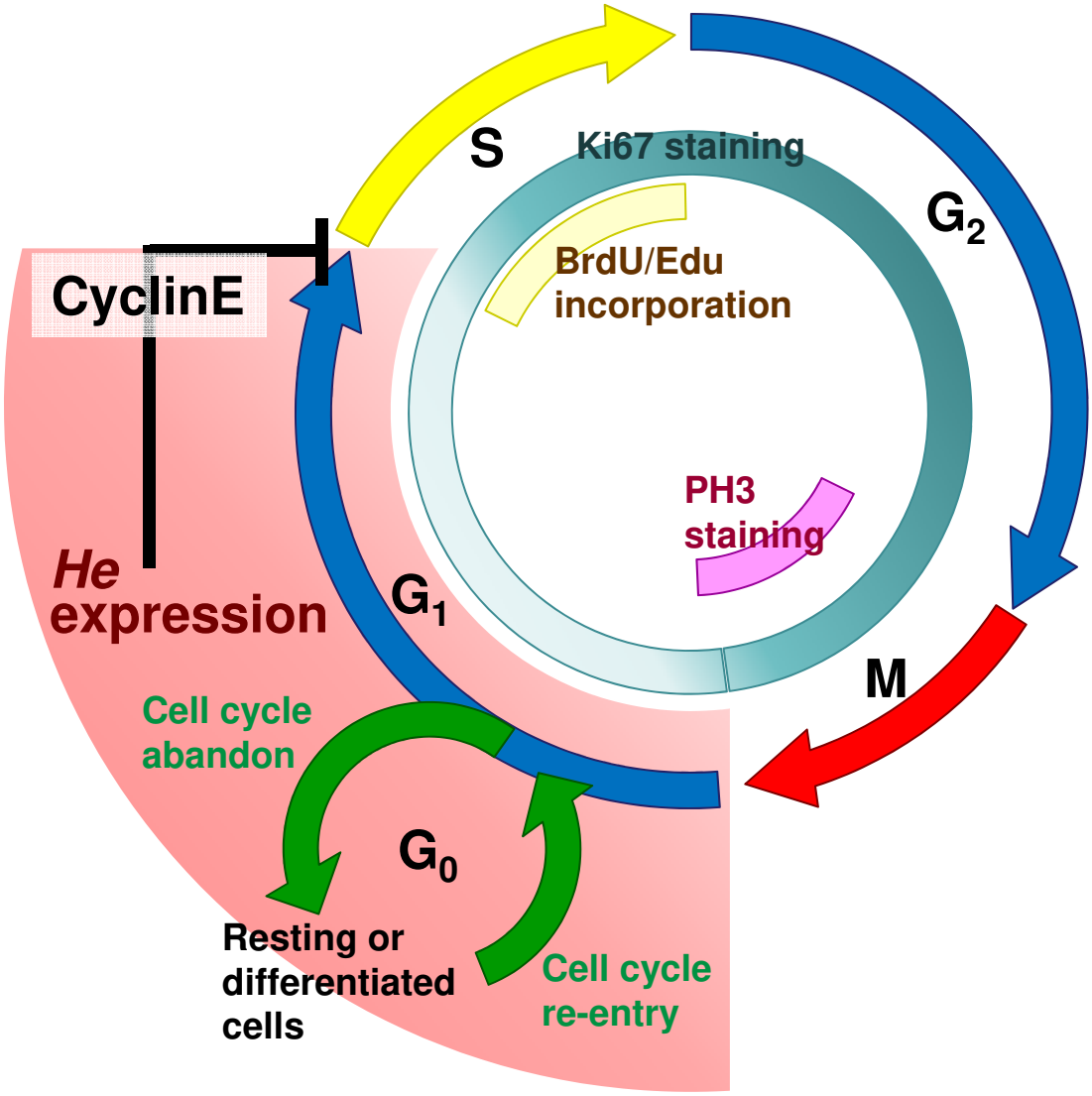

Figure S18. Schematic representation of He expression along NPCs cell cycle. Cell cycle phases are shown in different colors; G_0, green; G_1 blue; S, yellow; G_2, blue; and M, red. Inside circle and semicircles show the levels of Ki67 through cell cycle phases. Note that Ki67 immunostaining labels all phases except G_0 and the levels of expression are lower in phase G_1 (light blue); BrdU incorporation that labels S phase is represented in light yellow; and PH3 immunostaining that labels M phase in pink. Cells entering the phase G_0 abandon the cell cycle and become resting cells or postmitotic differentiated cells. However, resting cells can re-enter into the cell cycle. *He* is expressed in G_0 differentiated neurons and G_1 NPCs. In the later this transcription factor decrease Cyclin E to impair G_1-S phase transition and induce NPCs neuronal differentiation.

Development • Supplementary information